SUPPORTING INFORMATION

Covalent Triazine-based Frameworks – Switching Selectivity in HMF Photooxidation

Daniel Ditz[a], Nina M. Sackers[a], Felix Müller[b], Mirijam Zobel[b], Sebastian Bergwinkl[c], Patrick Nuernberger[c], Leonie Sophie Häser[a], Sarah Brettschneider[a], Florian M. Wisser[d], Christoph Bannwarth[e], and Regina Palkovits*[a,f]

a. *Dr. D. Ditz, Dr. N. M. Sackers, L. S. Häser, S. Brettschneider, Prof. R. Palkovits*
Heterogeneous Catalysis and Technical Chemistry,
Institute of Technical and Macromolecular Chemistry, RWTH Aachen University, Worringerweg 2, 52074 Aachen (Germany)
E-mail: palkovits@itmc.rwth-aachen.de
b. *Prof. M. Zobel*
Institute of Crystallography, RWTH Aachen University, Jägerstraße 17-19, 52066 Aachen, Germany;
c. *S. Bergwinkl, Prof. Dr. P. Nuernberger*
Institute of Physical and Theoretical Chemistry, University of Regensburg, Universitätsstr. 31, 93053 Regensburg, Germany;
d. *Dr. F. M. Wisser*
Erlangen Center for Interface Research and Catalysis (ECRC)
Friedrich-Alexander-Universität Erlangen-Nürnberg
Egerlandstraße 3, 91058 Erlangen (Germany)
e. *Prof. C. Bannwarth*
Theoretical Physical Chemistry of Large Molecules, Institute of Physical Chemistry, RWTH Aachen University,
Melatener Str. 20, 52074 Aachen (Germany)
f. *Prof. Dr. R. Palkovits*
Max-Planck-Institute for Chemical Energy Conversion
Stiftstr. 34-36, 45470 Mülheim an der Ruhr (Germany)

Table of contents

1. Methods and materials

1.1. Materials

All used reagents and solvents, their purity and the supplier are listed in the table below. 2,2,6,6-Tetramethylpiperidine (TEMP) was distilled over freshly activated zinc under reduced pressure prior to use.

Table S 1 : Reagents and solvents that were used for the synthesis, analysis and photocatalysis in this project.

Reagent or solvent	purity	supplier
1,4-Bezodimethanol	>99	abcr
2,2,6,6-Tetramethylpiperidine (TEMP)	>99	Sigma Aldrich
2,5-Furandicarbaldehyd	>99	Sigma Aldrich
2,5-Furandicarboxylic acid	>97	ChemPur
2,6-Naphthalenedicarboxylic acid	>95	Sigma Aldrich
5-(Hydroxymethyl)furfural	>97	fluoroChem
5-Formyl-2-furancarboxylic acid	>95	ChemPur
5-Hydroxymethyl-2-furancarboxylic acid	>95	ChemPur
5,5-Dimethyl-1-pyrroline N-oxide (DMPO)	for ESR spectroscopy	Sigma Aldrich
Acetone	>99.5	Chemsolute
Ammonium chloride	>99.7	Roth
Argon	>99.998	Westfalen
Benzene-1,4-dicarbonitrile	>98	Merck
Caesium carbonate	>99	Sigma Aldrich
Dimethyl sulfoxide (max. 0.025 % H2O)		Merck
Ethanol	>99.9	Chemsolute
Ethyl acetate	>99.5	Chemsolute
HCl in ethanol 2M		Kraft
Hydrochloric acid	>37	Chemsolute
Lithium aluminium hydride, 1.0 M solution in THF		Sigma Aldrich
Lithium bis(trimethylsilyl)amide, 1.0 M solution in THF		J&K
Methanol	>99.8	Chemsolute
Sulfuric acid	>97	Chemsolute
Synthtic air "KW-frei"	>99.99	Air Products
Tetrahydrofuran	>99.99	Chemsolute
Toluene	>99.8	Alfa Aesar

1.2. Experimental procedure for photocatalysis

All photocatalytic experiments were performed with a Peschl Ultraviolet MPDS Basic photocabinet equipped with a photoLAB Batch-S unit. In a typical catalysis CTF (12 mg) and HMF stock solution (6 mL, 0.01 M, natural pH) were added to a glass reactor in the dark and positioned in the photocabinet. The sample was equilibrated for one hour at 25 °C (temperature of cooling water) to ensure that the HMF adsorption equilibrium is reached (Table S 2). The catalysis was done under 460 nm light irradiation (35 mW cm^{-2}) and synthetic air pressure of 0.5 bar. Aliquots (200 µL) for analysis were withdrawn in fixed intervals and centrifuged to separate catalyst and aqueous reaction solution. The separated catalyst was washed with acetone (1 mL) to desorb potential adsorbates and centrifuged again for separation. Aqueous and organic supernatant were analysed separately via HPLC. Each catalysis was performed at least twice.

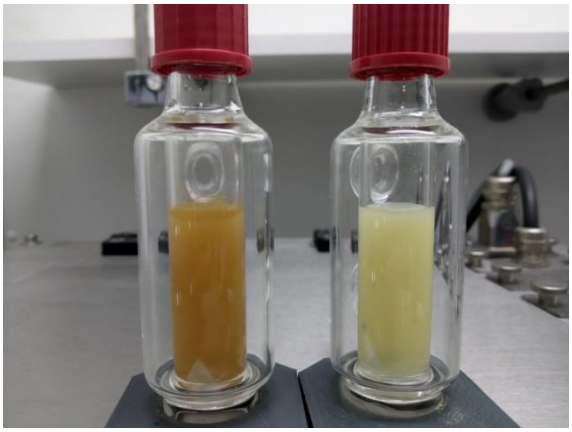

Figure S 1 : Picture of freshly dispersed CTF-2 (left) and CTF-1 (right) (12 mg each) in the reaction solution (6 mL).

1.2.1. Further photocatalytic experiments

Additional data are shown below to support some arguments, e.g. the yield of products from the direct oxidation pathway of HMF over CTF photocatalysts, the change in carbon balance over time and the influence of identical catalyst molar amount.

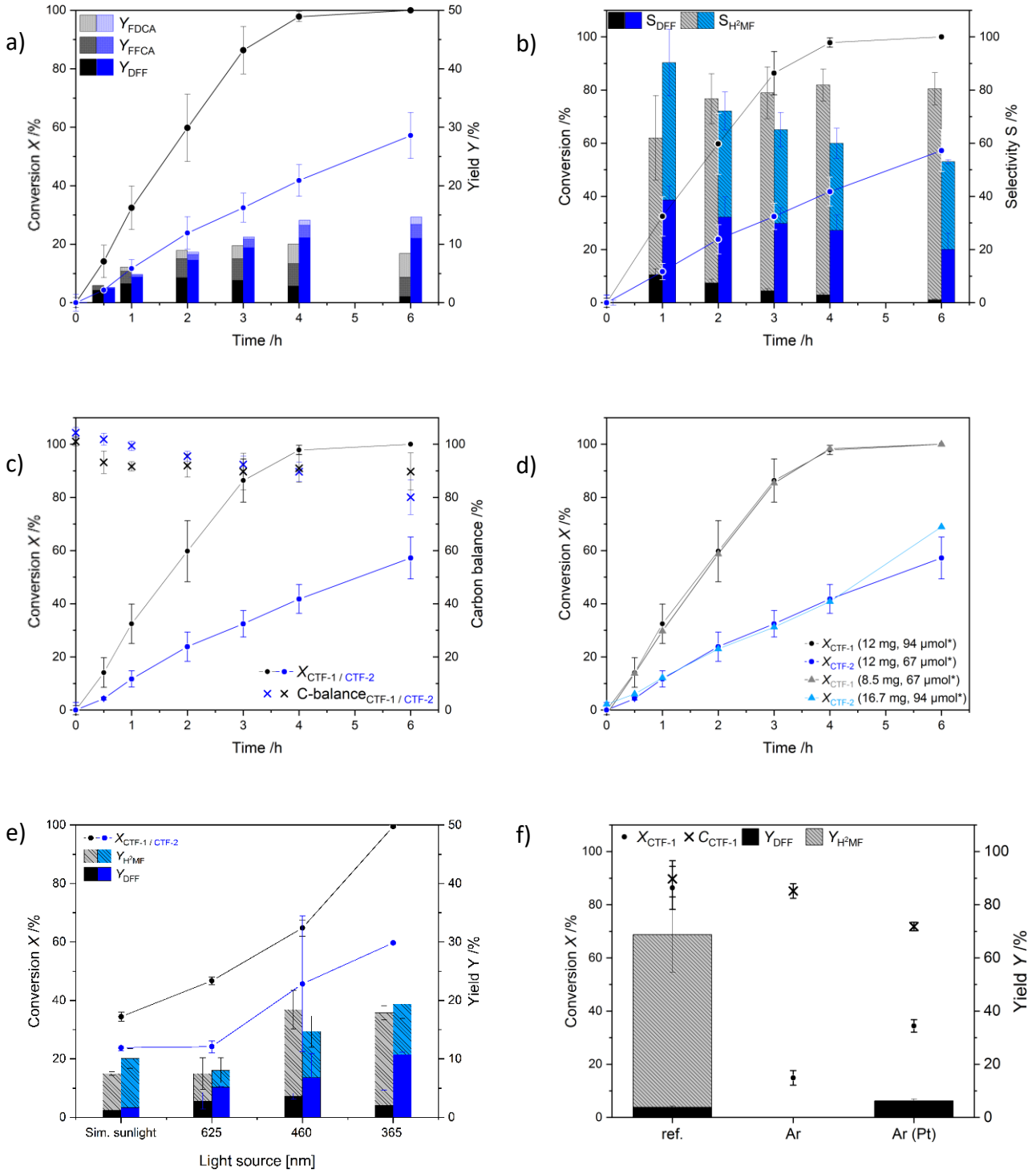

Figure S 2 : a) Photocatalytic direct oxidation of HMF over CTF-1 (black) or CTF-2 (blue). b) Photocatalytic oxidation of HMF over CTF-1 (black) and CTF-2 (blue) showing conversion and selectivity. c) Photocatalytic oxidation of HMF over CTFs showing conversion and carbon balance. d) Photocatalytic oxidation of HMF over CTFs with equivalent molar amount (*molar amount refers to the theoretical number of linker units). e) Photocatalytic oxidation of HMF over CTFs under different light irradiation. f) Photocatalytic oxidation of HMF over CTF-1 under synthetic air and argon atmosphere as well as Pt-CTF-1 under argon atmosphere after 3 h.

The direct oxidation pathway leads to an over oxidation of DFF to FFCA and FDCA (Figure S2a). No HMFA was detected. The carbon balance drops over time, although most products were quantified (Figure S2c). Non-identified side products (e.g. HKPA or oligomers of H^2MF) or incomplete washing of the catalyst contribute to the decrease in carbon balance. All catalytic experiments were performed with an identical mass concentration of the different CTFs for simplicity which in fact leads to a different molar amount of triazine and linker building blocks, in other words, different number of active sites and chromophores. However, reducing the amount of CTF-1 or increasing the amount of CTF-2 leads to no change in conversion (Figure S2d). This shows that both CTF dispersions absorb all incoming photons, thus the different molar amounts have no influence. All photocatalytic experiments were performed under 460 nm light irradiation which provides more energy than CTF-2's bandgap (CTF-2 direct bandgap of 2.63 eV or 470 nm) but less than CTF-1's bandgap (direct bandgap = 3.20 eV or 370 nm). Consequently, the valance electrons of CTF-1 may not be promoted to comparable excited singlet states which favour DFF formation. However, control experiments under multiple light sources (Figure S2e) show differences in activity but not in selectivity. Selectivity effects caused by the irradiation wavelength can therefore be excluded. Both catalysts are also active under simulated sunlight. H_2PtCl_6 (15 µL, 8 wt% solution in water) was added to a catalysis over CTF-1 under argon atmosphere to photo-deposit Pt-nanoparticles onto the CTF. In comparison to the catalysis without Pt-species, the conversion and yield of DFF is significantly increased (Figure S2f). This supports our hypothesis that hydrogen evolution as reductive half reaction couplet to HMF surface oxidation is theoretically possible over CTFs but kinetically hindered by hydrogen desorption. The reduced carbon balance indicates that Pt might also facilitate other reactions that led to unknown side products.
To study the influence of *tert*-butanol, used as hydroxyl radical scavenger, on the HMF adsorption, co-adsorption studies were conducted. Indeed, the amount of HMF adsorbed on the CTF surfaces decreases in the presence of *tert*-butanol. The reduced adsorption capacities may explain the slightly reduced catalytic activity observed in the control experiments in the presence of *tert*-butanol (Figure 3a).

Table S 2 : Adsorption experiments with CTF-1 and CTF-2 (12 mg) in HMF solution (6 mL, 0.01 M, natural pH) and HMF, tert-butanol solution (6 mL, 0.01 M HMF, 0.01 M *tert*-butanol, natural pH) after one hour.

Experiment	HMF adsorption /%	HMF capacity / mg/g
CTF-1 + HMF	16.1 $\pm$ 1.4	102 $\pm$ 9
CTF-1 + HMF + *tert*-butanol	14.1 $\pm$ 0.5	89 $\pm$ 3
CTF-2 + HMF	12.5 $\pm$ 1.2	79 $\pm$ 8
CTF-2 + HMF + *tert*-butanol	11.0 $\pm$ 0.2	69 $\pm$ 1

1.3. DFT and simplified TD-DFT calculations

Periodic density functional theory (DFT) calculations were carried out using the VASP program series (revision 5.4.4) [1,2] combined with the PBE exchange-correlation functional [3] within the generalized-gradient approximation (GGA). The PBE functional was complemented by the dDsC dispersion correction.[4] The electron-ion interactions were described by the PAW method. [5,6] In order to ensure accurate energies, the energy cut-off of the plane wave basis set was set to 400 eV. CTF-1 and CTF-2 were modelled as double layers in a 3D unit cell, in which the CTF layers are oriented perpendicular to the c direction. Slightly shifted AA stacking of the CTF layers is energetically more favourable for both CTFs and therefore considered in the following simulations. CTF-1 was simulated in a hexagonal cell with cell parameters of a = b = 14.55 Å and c = 6.69 Å leading to a CTF layer distance of 3.35 Å. For CTF-2, a monoclinic cell with a = 16.98 Å, b = 19.44 Å, c = 6.67 Å, α = β = 90°, γ = 120° and a layer distance of 3.34 Å were obtained. The Brillouin-zone was sampled by a Γ centered 3 x 3 x 3 Monkhorst-Pack grid [7] together with a Gaussian smearing with a width of 0.05 eV. Geometry optimizations were performed with convergence criteria for the self-consistent energy and the ionic relaxation of 10^{-6} eV and 0.02 eV $Å^{-1}$, respectively. The charge density distribution for VBM and CBM of both CTFs was calculated with a positive charge (+1) for VBM and a negative charge (-1) for CBM to approximate the electron-hole pair. VBM and CBM were determined from the band structure of the respective CTF. The aforementioned parameters were changed to a tetrahedron smearing with Blöchl corrections [8] and a denser k-point mesh of 9 x 9 x 9.

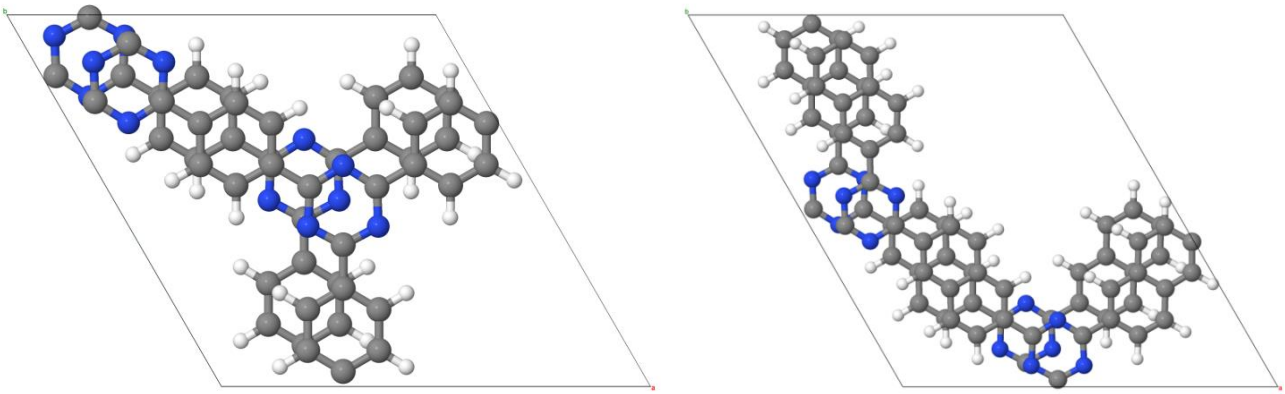

Figure S 3 : Visualization of optimized geometry of two CTF layers (left: CTF-1; right: CTF-2). Color Code: blue: nitrogen, gray: carbon, white: hydrogen. Front view along c direction.

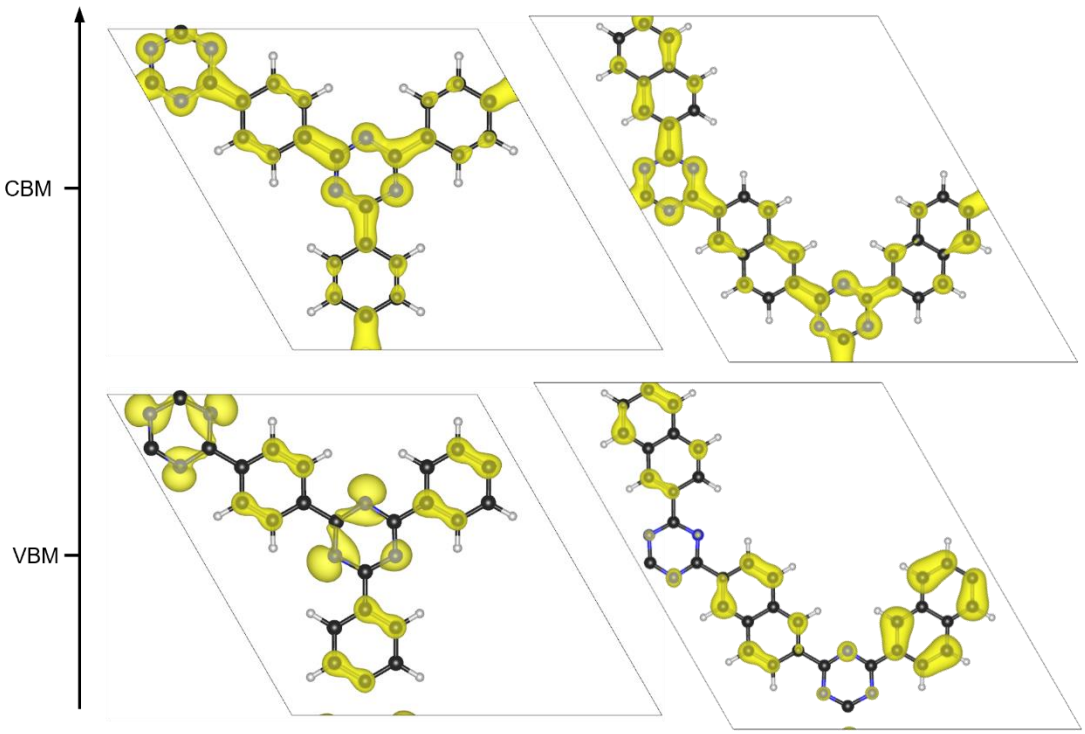

Figure S 4 : Visualization of charge density distribution for VBM and CBM of both CTFs for just one CTF layer (left: CTF-1; right: CTF-2). (Color Code: blue: nitrogen, gray: black, white: hydrogen. Front view along c direction.)

Cutouts were generated from the ground state minimum crystal geometries obtained as described above. For the cutouts, a single sheet of the CTF was taken and cropped to retain 9 ring frameworks, each encompassing six triazine rings. The cutouts were then capped with hydrogen atoms that were subsequently relaxed at the semiempirical GFN2-xTB level,[7] while keeping all carbon and nitrogen atoms fixed. The xtb program (version 6.4.0) was used for this purpose.[8] These cutouts are shown as inlets in Figure 4 of the main manuscript. The Cartesian coordinates of these cutouts are uploaded in a separate zip archive.

On these cutout geometries, excited state calculations for singlets and triplets were performed using the simplified Tamm-Dancoff-approximated time-dependent density functional theory (sTDA) approach[9] based on a ωB97X/def2-SV(P)[10] Kohn-Sham DFT reference. While the stda program[stdacode][11] has been used for the sTDA calculation, the GPU-accelerated quantum chemistry program TeraChem[terachem] has been used to carry out the preceding ground state calculation. All excitations up to 7 eV were considered and no shift was applied.[12]

For the generation of density-of-states plots, the state counts were convoluted with Gaussians with a width of 0.2 eV and normalized such that the lowest triplet peak maximum of the naphthyl CTF (CTF-2) has a value of one.

1.4. Characterisation of H^2MF

H^2MF was isolated by extracting most products out of the reaction solution (6 mL) with chloroform (10x 5 mL). After evaporation of the aqueous phase H^2MF remained as a yellowish syrup that quickly turned brown at room temperature. NMR experiments (^1H, quantitative ^{13}C, ^{13}C attached proton test (APT), heteronuclear multiple bond correlation (HMBC) and chemical ionization mass spectrometry (CI-MS) confirm the formation of H^2MF.

^1H NMR (400 MHz, DMSO-d6) δ 8.13 (s, formic acid), 7.56 (s, 1H), 7.39 (d, J = 5.6 Hz, 1H), 6.24 (d, J = 5.6 Hz, 1H), 5.19 (s, 1H), 3.56 (s, 2H). ^{13}C NMR (101 MHz, DMSO) δ 171.39 (Cq), 163.54 (formic acid), 155.49 (CH), 123.74 (CH), 108.51 (Cq), 63.92 (CH_2).

CI-MS 130 (H^2MF^+), 131 (H^2MF-H^+), 243 (condensed product), 261 (transition state to dimer $(H^2MF)_2$-H^+).

H^2MF cannot be acquired commercially, therefore HPLC calibration was performed with freshly produced H^2MF. After isolating the syrup, 10 mg were quickly weighed in and resolved in water (1.00 mL) to create a concentration series for HPLC calibration. Remaining syrup was weighed in with a known quantity of tetramethylsilane in acetone-d6 to check the H^2MF content of the syrup via NMR spectroscopy. We note that this method bares a larger error than our other HPLC calibrations since all other substances could be acquired commercially.

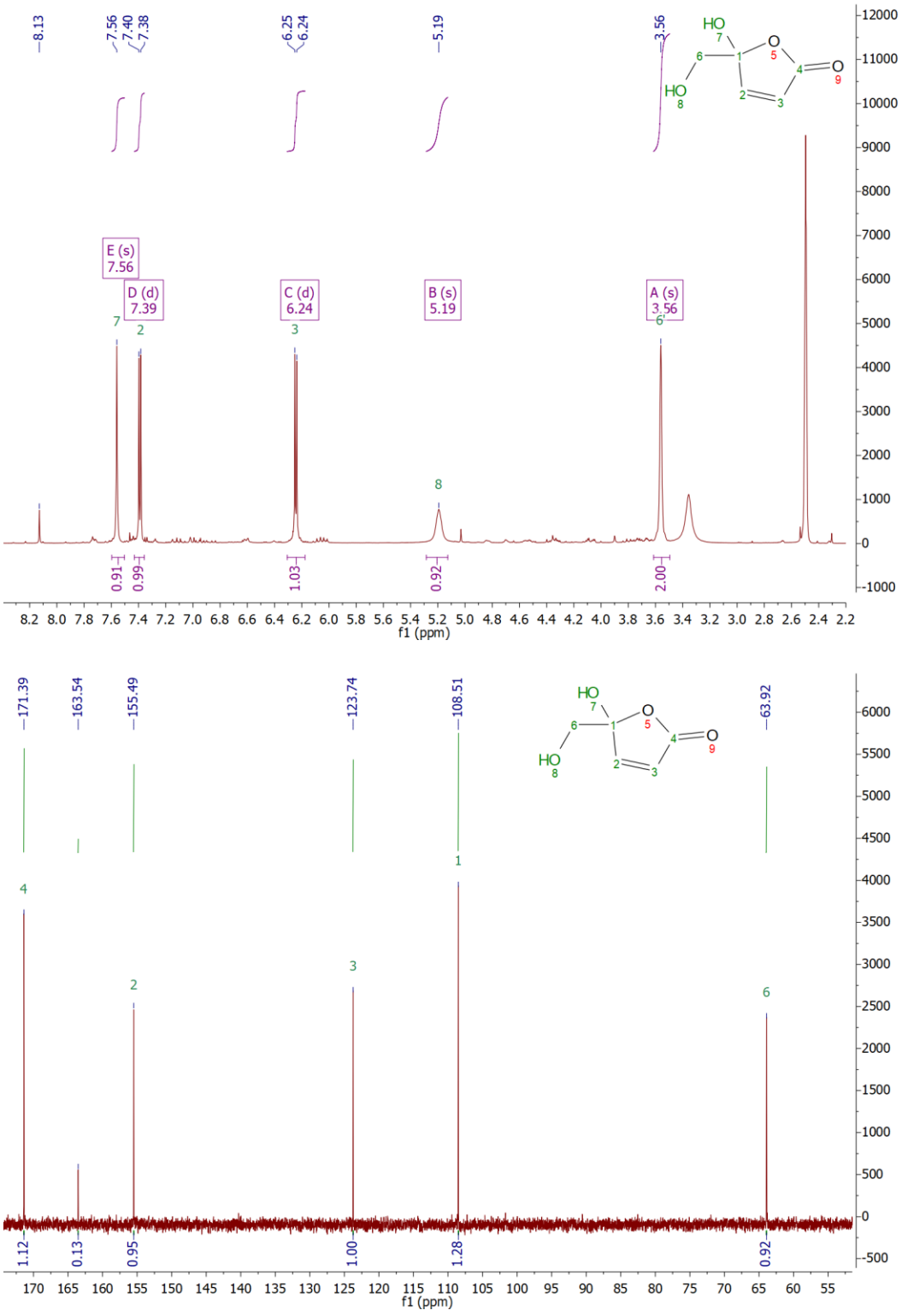

Figure S 5 : ^{1}H-NMR spectrum (top) and ^{13}C-NMR spectrum (bottom) of isolated H^{2}MF.

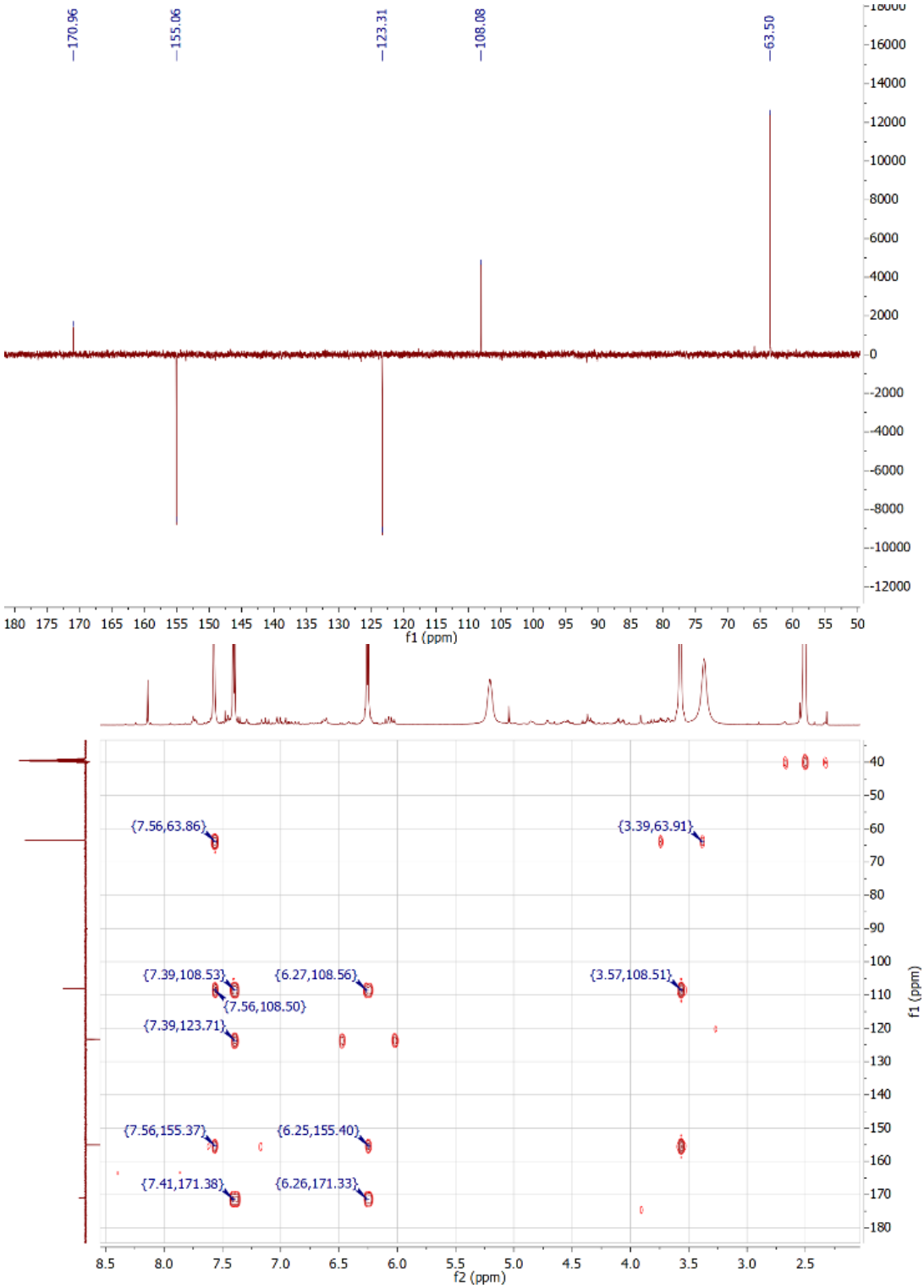

Figure S 6 : ^{13}C-APT-NMR spectrum (top) and ^{13}C,^{1}H-HMBC-NMR spectrum (bottom) of isolated H^{2}MF.

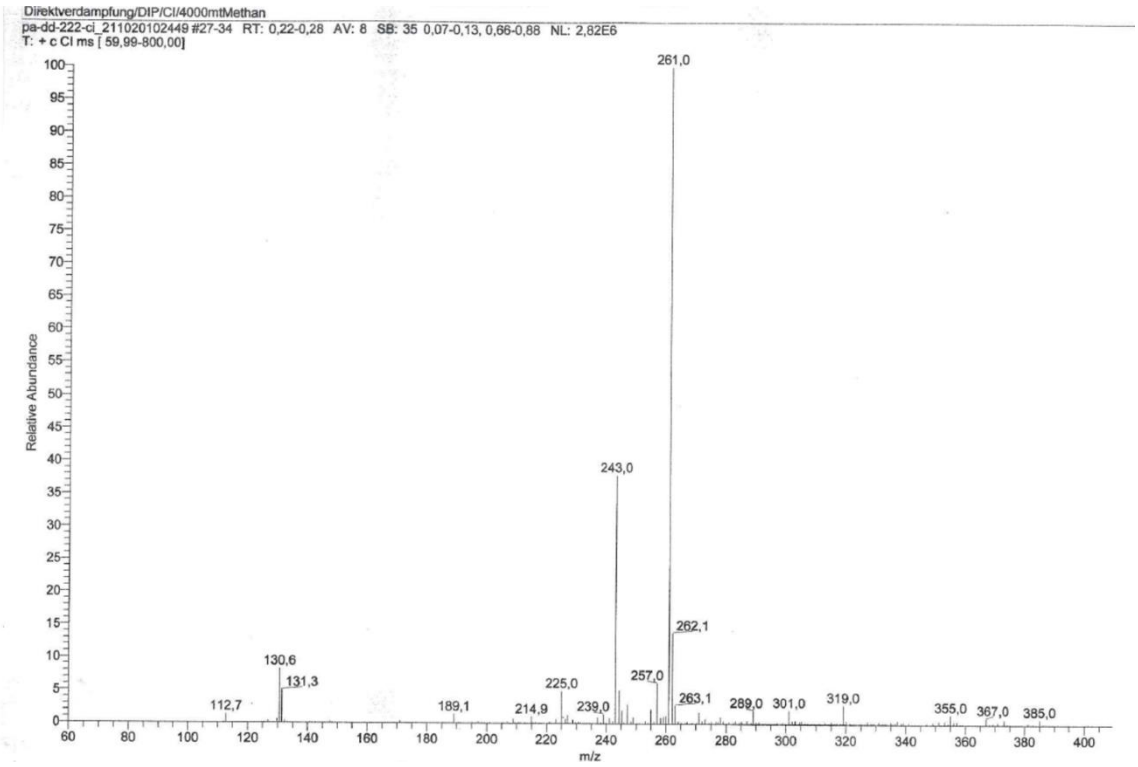

Figure S 7 : Chemical ionization spectrum of isolated H^2MF in methane after direct insertion.

2. Synthesis

2.1. Monomers

The synthesis of monomers was done according to (modified) literature procedure.

1) Terephthalamidine dihydrochloride[13]

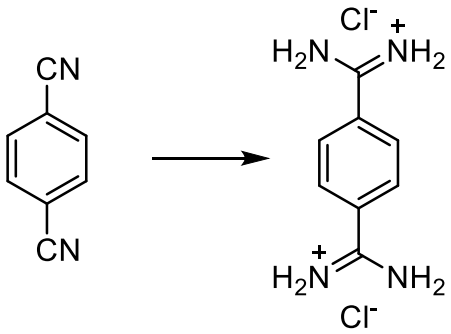

Benzene-1,4-dicarbonitrile (4.0 g, 31.2 mmol) was dissolved in dry THF (100 mL) under argon atmosphere. $LiN(SiMe_3)_2$ in THF (1 M, 100 mL) was added dropwise at 0 °C. The resulting solution was stirred for two hours at room temperature before it was cooled down again to 0 °C. The reaction was quenched by dropwise addition of HCl in EtOH (2 M, 200 mL) and the mixture was set aside overnight. Then, the precipitate was filtered, washed with EtOAc (3x 100 mL) and THF (3x 100 mL), and then the powder was recrystallized from a H_2O:EtOH (1:1) mixture (approx. 200 mL). Here, some insoluble impurities remained in solution upon clearing of the cloudy suspension which were separated by hot filtration. A brownish/yellow crystalline product precipitates from the filtered recrystallization mixture.

Yield: (1st recryst.: 4.36g, 18.6 mmol, 59.5 %, 2nd recryst. (80 mL): 0.78g, 3.3 mmol, 10.6%).
^{1}H NMR (300 MHz, DMSO-d6) δ 9.64 (s, 4H), 9.38 (s, 4H), 8.04 (s, 4H)

2) 2,6-Naphthalenediamidine dihydrochloride

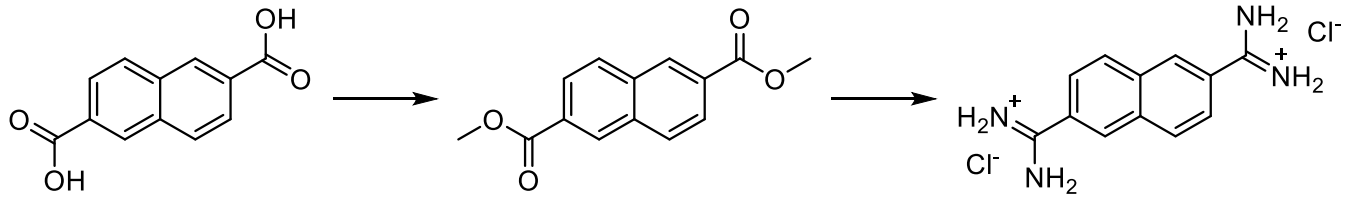

2.1) Dimethyl-2,6-naphthalenedicarboxylate

2,6-Naphthalenedicarboxylic acid (5.0 g, 23.13 mmol) was dispersed in methanol (100 mL) and H_2SO_4 (98 %, 4 mL) was added carefully before the solution was refluxed for 72 h. Next, the solvent was reduced and H_2O (50 mL) was added. The aqueous solution was extracted with ethyl acetate (3x 50 mL). After removal of the organic solvent the product was yielded as a white solid.

Yield: 5.4 g, 22.1 mmol, 96 %.
^{1}H NMR (400 MHz, DMSO-d6) δ 8.77 – 8.69 (m, 1H), 8.28 (d, J = 8.5 Hz, 1H), 8.07 (dd, J = 8.5, 1.6 Hz, 1H), 3.95 (s, 3H).
^{13}C NMR (101 MHz, DMSO-d6) δ 166.04, 134.18, 130.20, 129.10, 125.65, 52.46.

2.2) 2,6-Naphthalenediamidine dihydrochloride[14]

Ammonium chloride (50 mmol, 2.675 g, 10 equiv.) was dispersed in dry toluene (100 mL) and cooled to 0 °C. Trimethylaluminium in toluene (2 M, 25 mL, 10 equiv.) was added dropwise and the solution was stirred until no further gas evolution was visible. Next, dimethyl-2,6-naphthalenedicarboxylate (5 mmol, 1.23 g, 1 equiv.) was added and the solution was heated to 100 °C and stirred for 24 h. The reaction mixture was cooled down again to 0 °C and quenched by the addition of methanol (50 mL). The precipitate was filtered, washed with hot water (50 mL) and the filtrate was dried under reduced pressure at 60 °C. The residual solid was recrystallized from a H_2O:EtOH (1:1) mixture (approx. 75 mL) to yield the colourless product.

Yield: 0.97 g, 3.4 mmol, 68 %.
^{1}H NMR (400 MHz, DMSO-d6) δ 9.67 (s, 4H), 9.41 (s, 4H), 8.68 – 8.63 (m, 2H), 8.32 (d, J = 8.7 Hz, 2H), 7.99 (dd, J = 8.6, 1.8 Hz, 2H).
^{13}C NMR (101 MHz, DMSO) δ 165.98, 134.08, 130.39, 129.88, 128.63, 125.79.

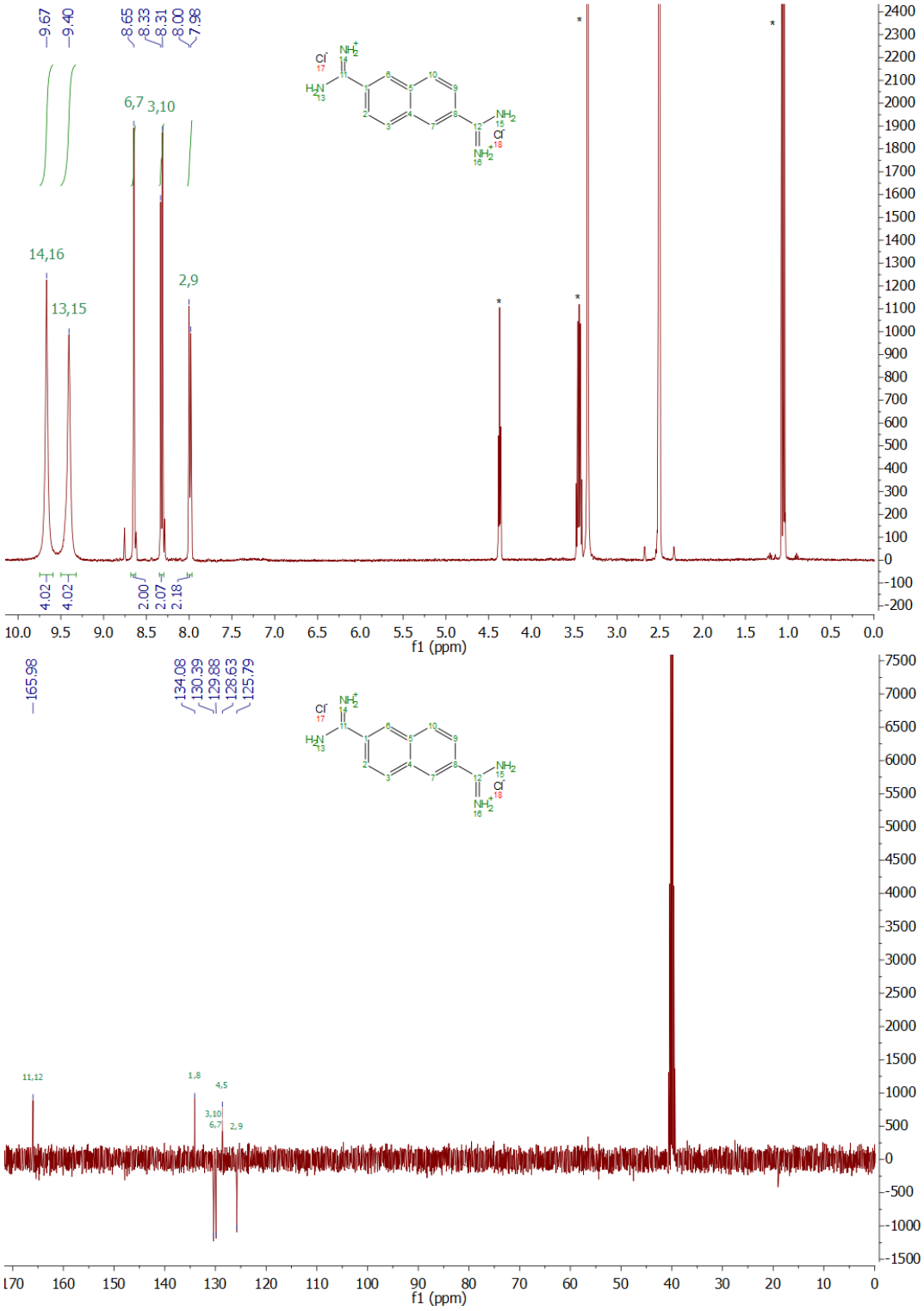

Figure S 8 : ^{1}H-NMR spectrum (top, impurities indicated with *) and ^{13}C-APT-NMR spectrum (bottom) of 2,6-Naphthalenedi-amidine dihydrochloride.

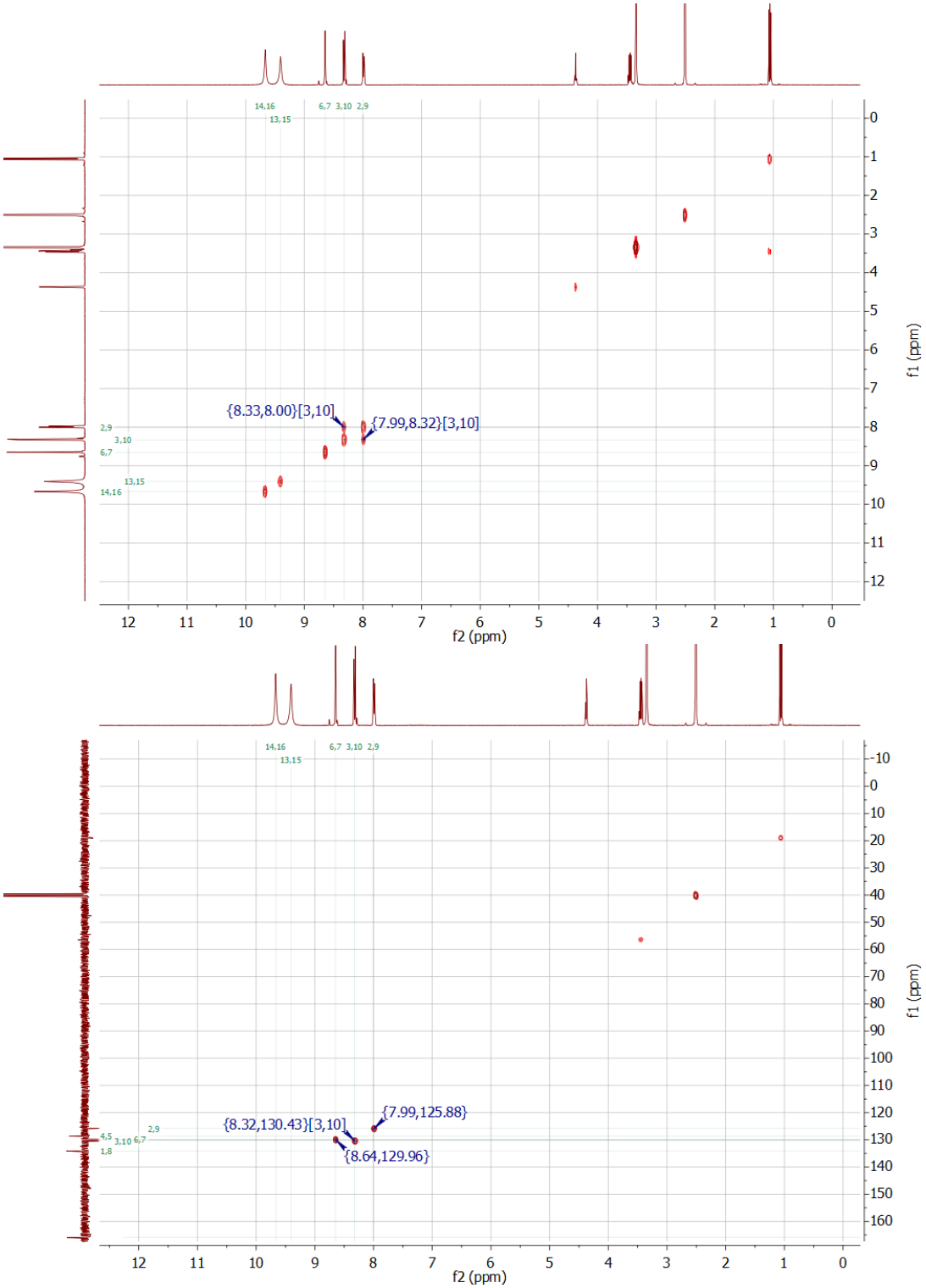

Figure S 9 : $^{1}H,^{1}H$-COSY-NMR spectrum (top) and $^{13}C,^{1}H$-HSQC-NMR spectrum (bottom) of 2,6-Naphthalenediamidine dihydrochloride.

3) 2,6-Bis(hydroxymethyl)naphthalene

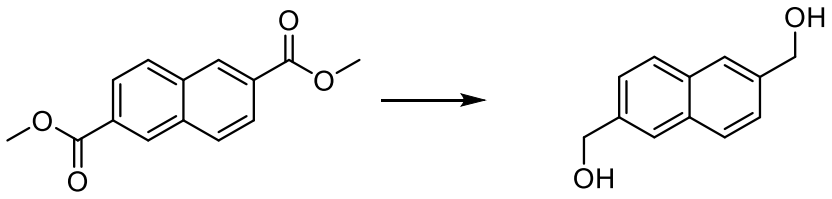

Dimethyl-2,6-naphthalenedicarboxylate (2.0 g, 8.2 mmol, 1 equiv.) was dissolved in dry THF (100 mL) under argon atmosphere. Lithium aluminium hydride in THF (1 M, 20 mL, 20 mmol, 2.5 equiv.) was added dropwise at room temperature over 1 h. The solution was stirred overnight before the reaction was quenched by the addition of methanol (30 mL) and aqueous HCl (1 M, 5 mL) at 0 °C. The solvent was evaporated, and the residual solid extracted with acetone (3x 50 mL). The organic solvent was evaporated, and the product was recrystallized from acetone (approx. 100 mL).

Yield: 1.54 g, 8.2 mmol, 99 %.
^{1}H NMR (400 MHz, DMSO-d6) δ 7.84 (d, J = 8.3 Hz, 2H), 7.81 – 7.78 (m, 2H), 7.45 (dd, J = 8.4, 1.6 Hz, 2H), 5.30 (t, J = 5.7 Hz, 2H), 4.65 (d, J = 5.6 Hz, 4H).
^{13}C NMR (101 MHz, DMSO-d6) δ 140.16, 132.52, 127.89, 125.83, 124.67, 63.49.

2.2. Covalent Triazine Frameworks

The synthesis of CTFs was done according to a modified literature procedure.[13]

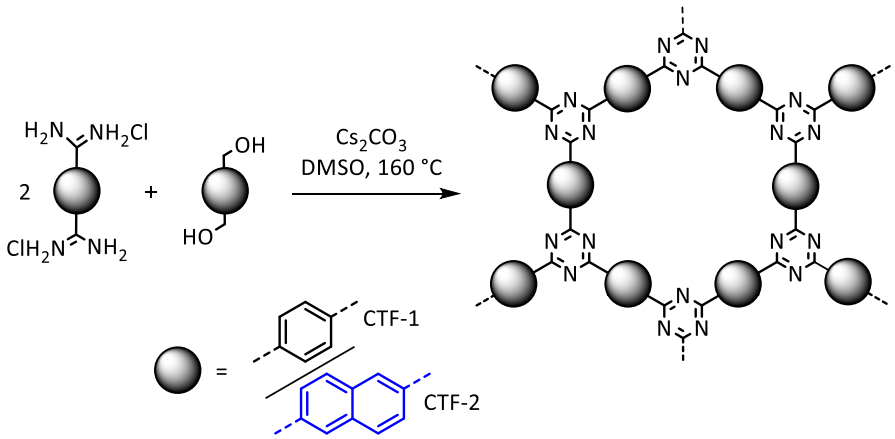

Figure S 10. Reaction scheme for CTF synthesis.

CTF-1

1,4-Benzenedimethanol (1.116 g, 8.08 mmol, 1 equiv.), terephthalamidine dihydrochloride (3.8 g, 16.16 mmol, 2 equiv.) and Cs_2CO_3 (11.583 g, 35.55 mmol, 4.4 equiv.) were dispersed in dry dimethyl sulfoxide (250 mL) under argon atmosphere. The mixture was heated to 100 °C and stirred for 24 h, before increasing the temperature for an addition 36 h to 160 °C. The reduced temperature compared to literature (180 °C) reduces the amount of sulphur species incorporated into the network.[15] After the reaction mixture was cooled to RT, the precipitate was isolated by filtration, washed with aqueous HCl (1 M, 3x 100 mL), H_2O (3x 100 mL), ethanol (3x 100 mL), THF (3x 100 mL) and dried under vacuum.

Yield: 3.16 g (91 %).
CHN analysis: experimental: C: 69.3 %, H: 3.5 %, N: 20.4 %, calculated for 100% conversion: C: 75.0 %, H: 3.1 %, N: 21.9 %
C/N molar ratio: 3.96 (calculated 4)

CTF-2

2,6-Bis(hydroxymethyl)naphthalene (188.2 mg, 1.0 mmol, 1 equiv.), 2,6-naphthalenediamidine dihydrochloride (570.3 mg, 2.0 mmol, 2 equiv.) and Cs_2CO_3 (1.433 g, 4.4 mmol, 4.4 equiv.) were dispersed in dry dimethyl sulfoxide (30 mL) under argon atmosphere. The mixture was heated to 100 °C and stirred for 24 h, before increasing the temperature for an addition 36 h to 160 °C. After the reaction mixture was cooled to RT, the precipitate was isolated by filtration, washed with aqueous HCl (1 M, 3x 25 mL), H_2O (3x 25 mL), ethanol (3x 25 mL), THF (3x 25 mL) and dried under vacuum.

Yield: 238 mg (41 %).

CHN analysis: experimental: C: 73.4 %, H: 3.4 %, N: 14.5 %, calculated for 100% conversion: C: 80.9 %, H: 3.4 %, N: 15.7 % C/N molar ratio: 5.91 (calculated 6)

3. Characterization of the materials

3.1. Electrochemical & Photoelectrochemical analysis

All (photo-) electrochemical measurements were performed with a three-electrode set-up from Metrohm (Autolab PGSTAT204), using a Pt counter electrode and a Ag/AgCl (3 M NaCl) reference electrode. The working electrode was fabricated by mixing under sonication 5 mg CTF (particle size <40 µm) with water, ethanol (50 µL each) and 1 wt% Nafion solution for 30 mins. Then, 2 µL of the suspension was drop casted onto 0.25 cm² of a FTO substrate and dried under ambient conditions. Spare FTO surface was covered with an isolating paint. The sample was first conditioned via 25 CV cycles between -0.3 V and 1.2 V (100 mV s^{-1}) before any analysis and the open circuit potential (OCP) was measured in the dark. Mott-Schottky measurements were conducted in the dark in Na_2SO_4 (2 M in water) electrolyte between -0.3 V and 1.1 V in 0.05 V steps at three different frequencies (400, 700, 1000 Hz). Prior, the isoelectric point was determined with a Malvern Panalytical Zetasizer Ultra equipped with an MPT-3 autotitrator via Zeta-potential measurements. Therefore, 10 mg CTF was sonicated for 1 h in 30 mL aqueous NaCl (10 mM in Milli-Q water, previously purged with argon), filtered through a 1.2 µm syringe filter and subsequently 15 mL were used for one Zeta-potential titration measurement. The pH was adjusted either to acidic or basic values using aqueous HCl (0.01 M) or aqueous NaOH (0.01 M) respectively, starting each time from the natural pH to minimize the salt loading. During the measurement the solution was continuously purged with argon. The isoelectric point for both materials is around pH 5.5. EIS analysis was conducted in aqueous HMF solution (0.01 M, natural pH) at OCP potential under illumination from the back (365 nm, 1 W m^{-2}). Photocurrent measurements were also performed in aqueous HMF solution (0.01 M, natural pH) at OCP potential under periodical illumination from the back (60 s intervals, 365 nm, 1 W m^{-2}). All (photo-) electrochemical measurements were performed at least three times.

The following simplified Randles circuit was used to fit impedance data.

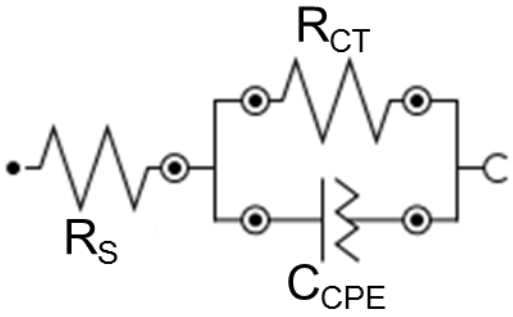

Z = Impedance (Ω); R_S = electrolyte resistance (Ω); R_{CT} = charge transfer resistance (Ω); C_{CPE} = constant phase element (F)

$$Z_{R_s} = R_S \; ; \; Z_{R_{CT}} = R_{CT} \; ; \; Z_{C_{CPE}} = \frac{1}{Y_0 \omega^a e^{\frac{\pi}{2} a \, i}}$$

$$Z = Z' + i\,Z'' = R_S + \frac{R_{CT}}{1 + R_{CT} Y_0 \omega^a e^{\frac{\pi}{2} a \, i}}$$

$$Z = R_S + \frac{R_{CT}}{1 + R_{CT} Y_0 \omega^a \cos\frac{\pi}{2} a + i\, R_{CT} Y_0 \omega^a \sin\frac{\pi}{2} a} \cdot \left(\frac{1 + R_{CT} Y_0 \omega^a \cos\frac{\pi}{2} a - i\, R_{CT} Y_0 \omega^a \sin\frac{\pi}{2} a}{1 + R_{CT} Y_0 \omega^a \cos\frac{\pi}{2} a - i\, R_{CT} Y_0 \omega^a \sin\frac{\pi}{2} a} \right)$$

$$Z = R_S + \frac{R_{CT} + R_{CT}^2 Y_0 \omega^a \cos\frac{\pi}{2} a - i\, R_{CT}^2 Y_0 \omega^a \sin\frac{\pi}{2} a}{1 + 2\, R_{CT} Y_0 \omega^a \cos\frac{\pi}{2} a + R_{CT}^2 Y_0^2 \omega^{2a}}$$

$$\Rightarrow Z' = R_S + \frac{R_{CT} + R_{CT}^2 Y_0 \omega^a \cos\frac{\pi}{2} a}{1 + 2\, R_{CT} Y_0 \omega^a \cos\frac{\pi}{2} a + R_{CT}^2 Y_0^2 \omega^{2a}}$$

$$\Rightarrow -Z'' = \frac{R_{CT}^2 Y_0 \omega^a \sin\frac{\pi}{2}a}{1 + 2\,R_{CT} Y_0 \omega^a \cos\frac{\pi}{2}a + R_{CT}^2 Y_0^2 \omega^{2a}}$$

Table S3 : Results of the equivalent circuit circle fit.

	run	Y_0 /µF	R_{CT} /kΩ	R_S /kΩ	a
CTF-1	1	5.34	1092	8.6	0.84
	2	5.30	903	9.4	0.79
	3	6.10	915	12.6	0.78
	average	5.6 ± 0.4	970 ± 90	10 ± 2	0.80 ± 0.03
CTF-2	1	3.25	3592	0.3	0.86
	2	5.22	2450	2.9	0.77
	3	4.75	1933	1.7	0.79
	average	4.4 ± 0.8	2700 ± 700	1.6 ± 1.1	0.81 ± 0.04

	run	Y_0 /µF	R_{CT} /kΩ	R_S /kΩ	a
CTF-1	1	5.34	1092	8.6	0.84
	2	5.30	903	9.4	0.79
	3	6.10	915	12.6	0.78
	average	5.58 ± 0.37	970 ± 86	10.2 ± 1.7	0.80 ± 0.03
CTF-2	1	5.22	2450	3.0	0.77
	2	4.75	1933	1.8	0.79
	average	4.99 ± 0.24	2192 ± 259	2.4 ± 0.6	0.78 ± 0.01

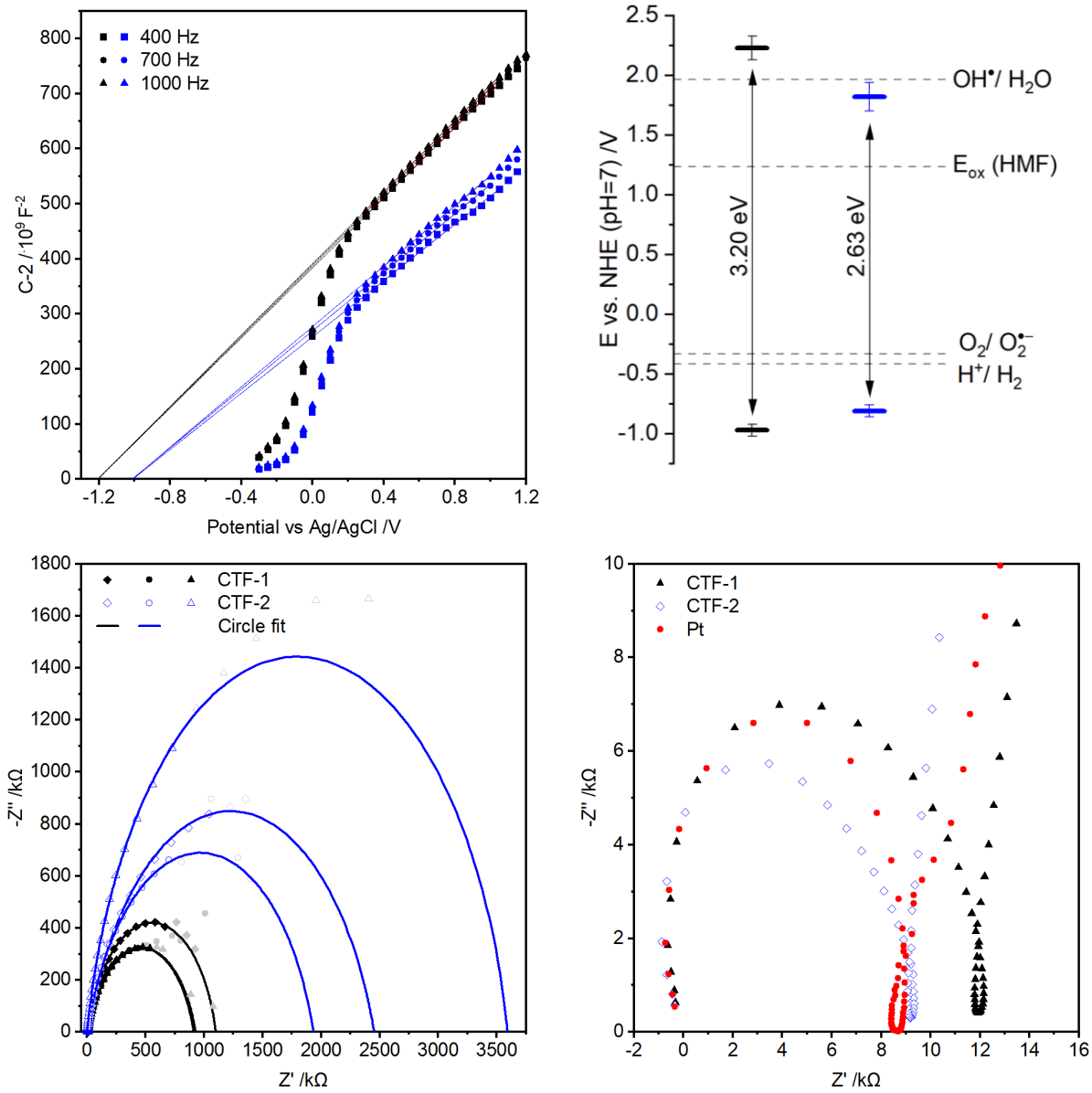

Figure S 11 : Mott-Schottky analysis (top left) and band alignment of CTF materials and relevant redox potentials versus normal hydrogen electrode (NHE) potential at reaction pH (top right) of CTF-1 (black) and CTF-2 (blue) and Nyquist diagrams of CTFs and Platinum (bottom).
In the EIS analysis a smaller semicircle occurs before the semicircle of the CTF is detected. Zooming in and comparing the arc with a measurement of two platinum electrodes reveals that this first semicircle results from processes at the platinum electrode.

3.2. Elemental analysis

An Elementar vario EL cube was used to determine the CHN composition of the materials by combustion analysis at the institute of organic chemistry at RWTH Aachen.

3.3. Emission spectroscopy

Steady state emission and excitation spectra were recorded on a Fluorolog 3-22 spectrometer (Horiba Jobin Yvon) equipped with a multichannel scaler PCI card from FAST ComTec (time resolution 250 ps). Dry samples were measured in sealed quartz ampoules under inert atmosphere at room temperature. Suspensions of 0.1 mg/1 mL in water were measured in 10 mm quartz fluorescence cuvettes. To avoid sedimentation during the measurements the suspensions were stirred. Prior to measurement the CTFs were degassed at 80°C over night, water was degassed by three cycles of freeze-pump-thaw, the suspensions were prepared under Ar atmosphere, and the cuvette sealed under inert conditions. For measurements after exposure to O_2, the suspensions were saturated inside the cuvette by bubbling O_2 through it for 1h at room temperature. The nanosecond emission decay of the solid samples under Ar was measured by time-correlated single photon counting (TCSPC) using the same Fluorolog 3-22 spectrometer. The fluorescence was excited at 378 nm using a pulsed diode laser (Picobrite PB-375L, pulse width < 100 ps). A series of TCSPC decay curves were recorded in the emission range from 450 to 700 nm with an increment of 10 nm.

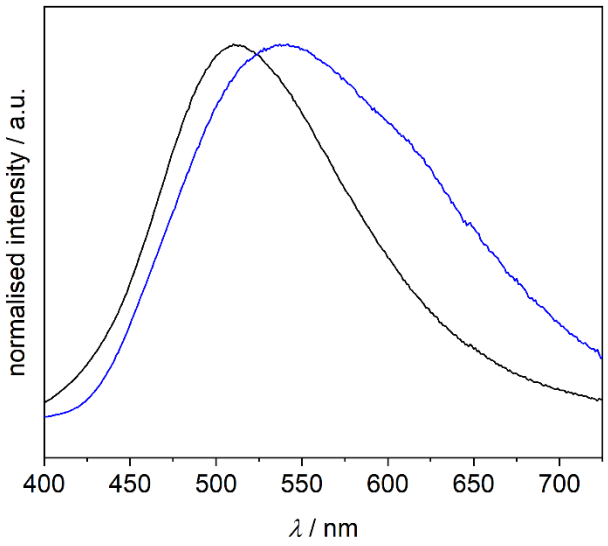

Figure S 12 : Normalised steady state emission spectra of CTF-1 (black) and CTF-2 (blue) after excitation at 378 nm.

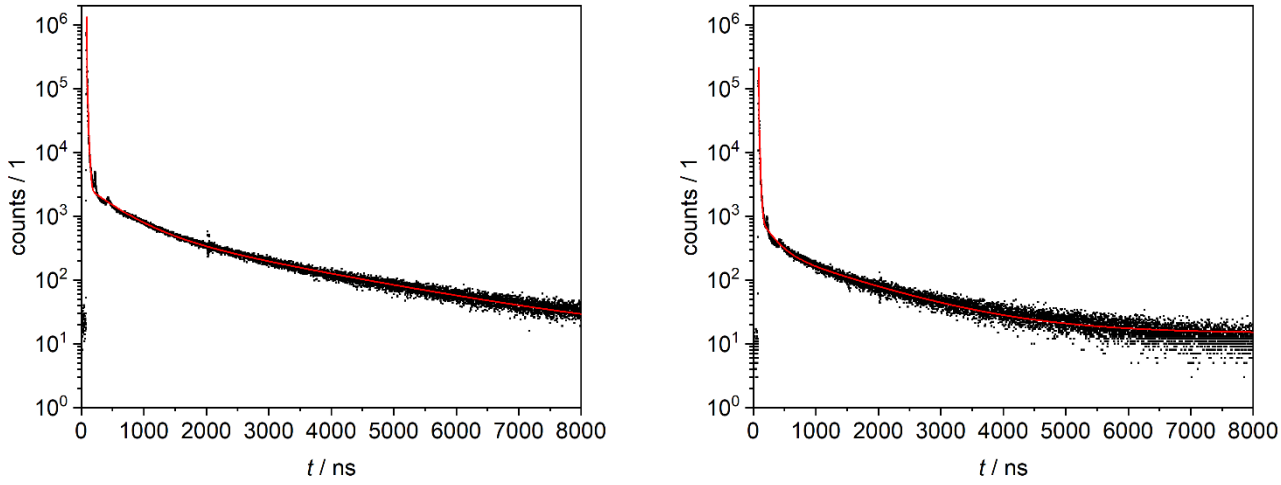

Figure S 13 : TCSPC decay curves of CTF-1 recorded in the solid state at different detection wavelengths recorded upon photoexcitation at 378 nm. Left: λ_{em}= 510 nm and Right: λ_{em}= 600 nm.

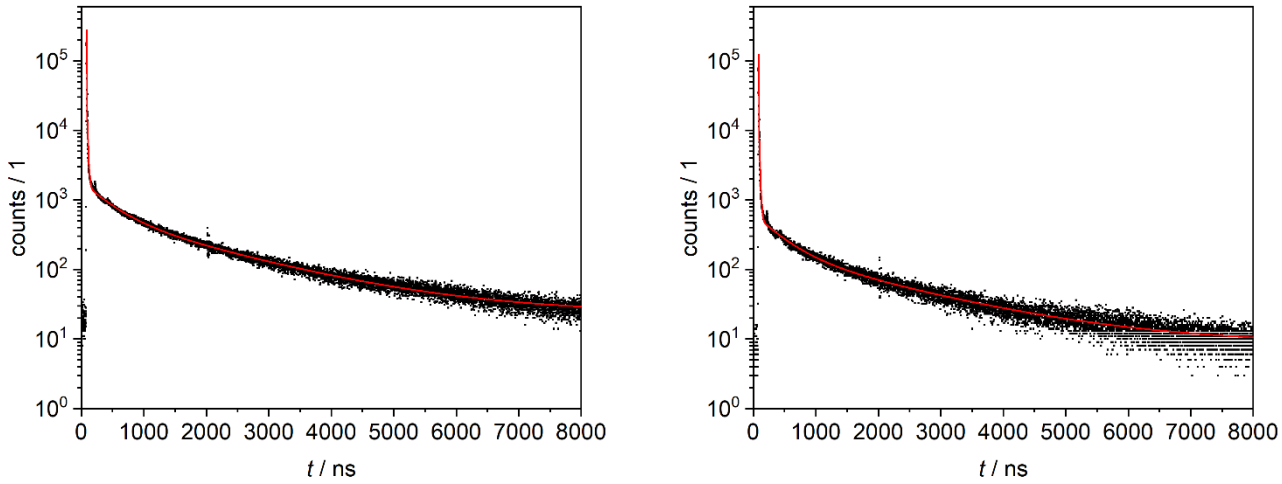

Figure S 14 : TCSPC decay curves of CTF-2 recorded in the solid state at different detection wavelengths recorded upon photoexcitation at 378 nm. Left: λ_{em}= 540 nm and Right: λ_{em}= 600 nm.

Table S4 : Fit parameters of the TCSPC decays for CTF-1 and CTF-2

	CTF-1		CTF-2	
λ_{em}	decay components	emission contribution [b]	decay components	emission contribution [b]
510 nm (CTF-1) / 540 nm (CTF-2)	τ_1: 2.0 ns (78.2 %) [a]	21.0 %	τ_1: 1.6 ns (87.0 %)	13.2 %
	τ_2: 14.4 ns (21.5 %)	42.2 %	τ_2: 14.2 ns (12.2 %)	16.6 %
	τ_3: 500 ns (0.2 %)	15.4 %	τ_3: 399 ns (0.5 %)	20.1 %
	τ_4: 2.2 µs (0.1 %)	21.3 %	τ_4: 1.7 µs (0.3 %)	50.1 %
600 nm	τ_1: 2.3 ns (73.4 %)	19.9 %	τ_1: 1.9 ns (87.0 %)	21.2 %
	τ_2: 14.4 ns (26.0 %)	42.1 %	τ_2: 13.8 ns (12.5 %)	21.6 %
	τ_3: 199 ns (0.4 %)	10.2 %	τ_3: 401 ns (0.4 %)	18.5 %
	τ_4: 1.3 µs (0.2 %)	27.8 %	τ_4: 1.8 µs (0.2 %)	38.7 %

a) Relative amplitude contribution to the decay. b) Relative contribution to the steady state emission calculated by using the product of the lifetime by the amplitude.

Table S5 : Averaged time constants and emission contribution for the short lived ($\bar{\tau}_{\mathrm{fluor}}$) and long lived ($\bar{\tau}_{\mathrm{phos}}$) emissive state CTF-1 and CTF-2 as solid under argon atmosphere.

	CTF-1		CTF-2	
λ_{em}	decay components	emission contribution	decay components	emission contribution
510 nm (CTF-1) / 540 nm (CTF-2)	$\bar{\tau}_{\mathrm{fluor}}$: 10 ns [a] (99.7 %)	63.3 %	$\bar{\tau}_{\mathrm{fluor}}$: 9 ns (99.2 %)	29.8 %
	$\bar{\tau}_{\mathrm{phos}}$: 1.7 µs (0.3 %)	36.7 %	$\bar{\tau}_{\mathrm{phos}}$: 1.3 µs (0.8 %)	70.2 %
600 nm	$\bar{\tau}_{\mathrm{fluor}}$: 11 ns (99.4 %)	62.0 %	$\bar{\tau}_{\mathrm{fluor}}$: 8 ns (99.5 %)	42.8 %
	$\bar{\tau}_{\mathrm{phos}}$: 1.0 µs (0.6 %)	38.0 %	$\bar{\tau}_{\mathrm{phos}}$: 1.4 µs (0.5 %)	57.2 %

a) The average lifetime ($\bar{\tau}$) was calculated by the formula $\bar{\tau} = (\alpha_i\tau_i^2 + \alpha_j\tau_j^2)/(\alpha_i\tau_i + \alpha_j\tau_j)$ with the relative amplitude contributions α and τ the corresponding lifetimes ($i = 1, j = 2$ for $\bar{\tau}_{\mathrm{fluor}}$ and $i = 3, j = 4$ for $\bar{\tau}_{\mathrm{phos}}$).[15]

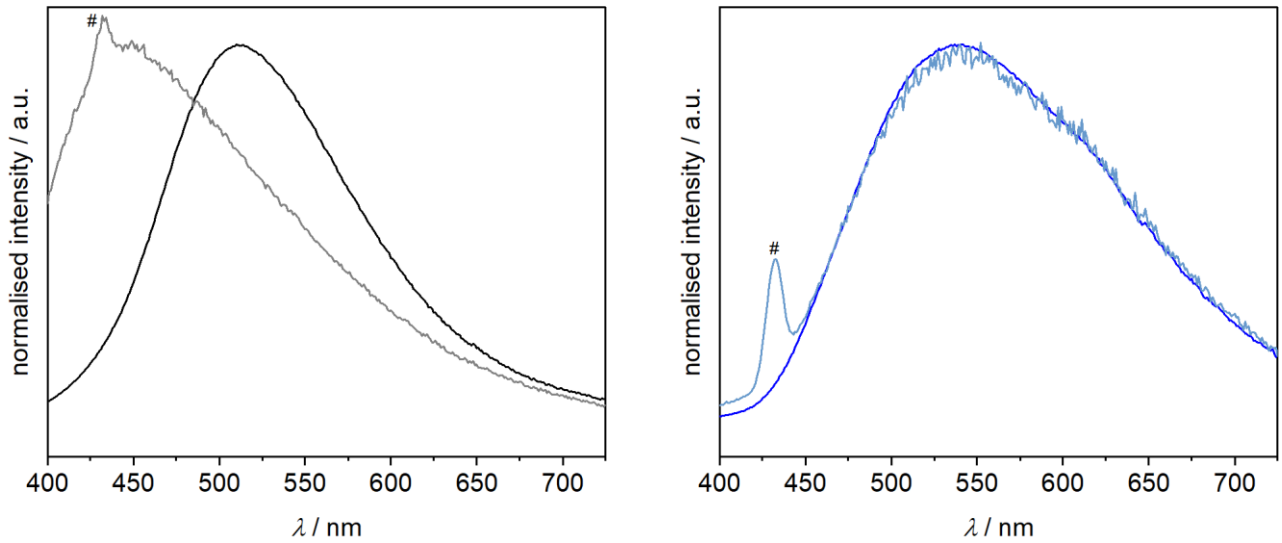

Figure S 15 : Left: Steady state emission spectra of CTF-1 after excitation at 378 nm in the solid state (black) and dispersed in water (gray). Right: Steady state emission spectra of CTF-2 after excitation at 378 nm in the solid state (dark blue) and dispersed in water (light blue). # denotes RAMAN signal of water (O-H stretch).[16,17]

3.4. EPR analysis

EPR analysis on suspensions of CTFs were conducted on a MiniScope MS 400 X-band CW EPR spectrometer (Magnettech, Freiberg instruments) at 9.5 GHz (50 – 650 mT). For in-situ EPR experiments the suspensions were illuminated with a blue LED (455 nm) inside the EPR cavity. Spectra were recorded applying a B_0 sweep width of 50 mT, a modulation amplitude of 0.2 mT and a microwave attenuation of 10 dB. For time resolved in situ EPR investigation, the LED lamp was switch on after the first spectrum was measured and EPR spectra were recorded every two minutes for up to 20 minutes (sweep time 30 s, time between two sweeps 90 s). In case of control experiments with P25 titanium dioxide the suspension was illuminated with a Lightningcure Spot light source LC8 (Hamamatsu).

The samples were freshly prepared before the EPR experiments. Briefly, 0.1M solutions of DMPO (Sigma Aldrich, for EPR) and TEMP (Sigma Aldrich, 99 %) were prepared using oxygen saturated distilled water. 1 ml of the scavenger solution was added to 1 mg of CTF, the suspension directly transferred to the glass ampoules and measured at RT. In case of experiments in presence of HMF, the solutions were 0.1M in scavenger and 0.01M in HMF.

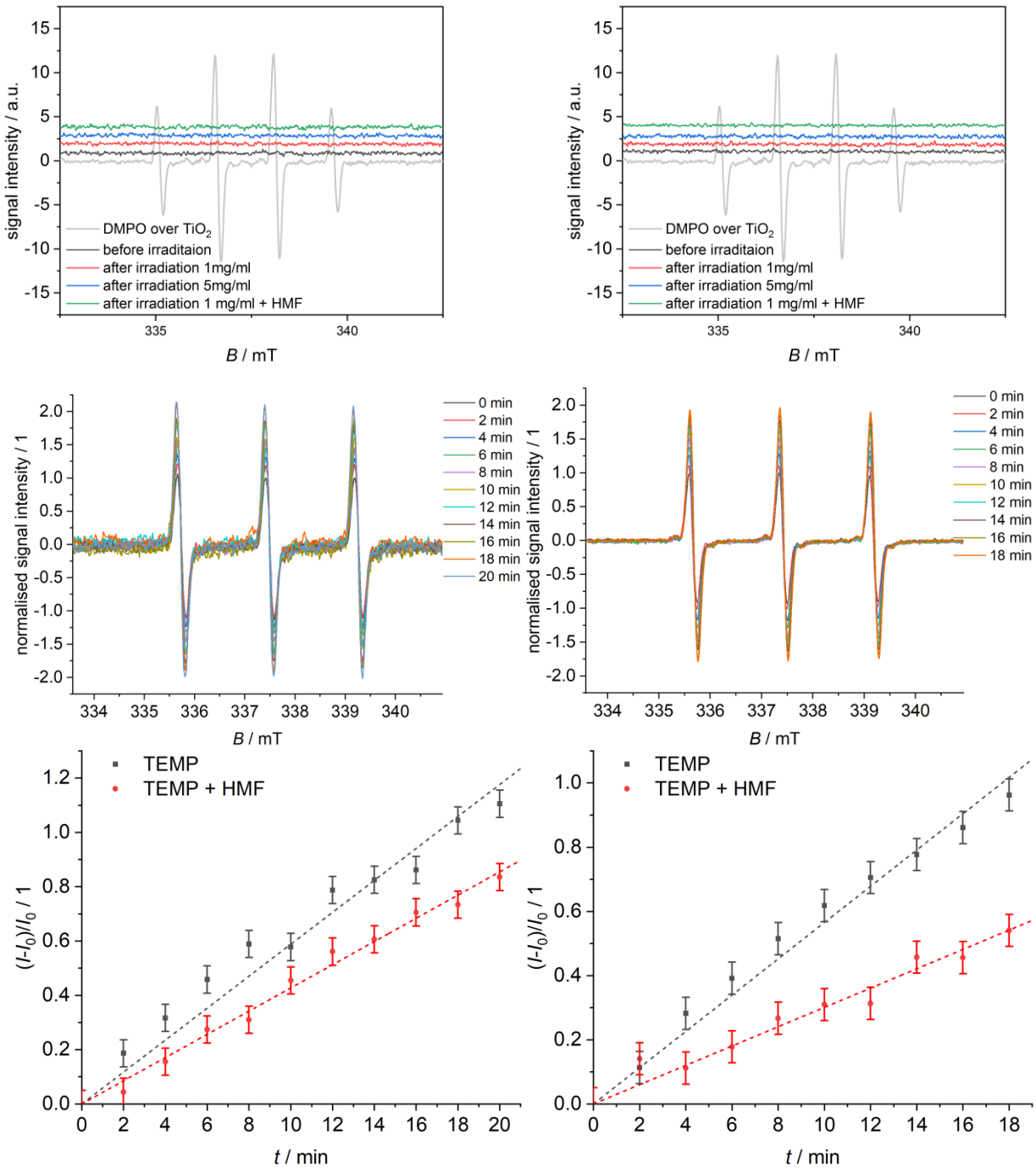

Fig. S16:

Figure S 16 : EPR studies on DMPO and TEMP.

3.5. HPLC

HPLC was conducted on a Shimadzu Prominence UFLC device, equipped with a refractive index detector and a UV-VIS detector. Two organic acid resin columns (PS-DVB copolymer, 300 mm x 8 mm and 100 mm x 8 mm) from CS-Chromatographie Service were used with trifluoroacetic acid in water as eluent (2 mM,1 mL min^{-1}) at 40 °C. The columns were operated in parallel, controlled via a column selection valve (column switch after 7 min retention time pre-column), to speed up analysis. HMF and DFF were calibrated on the short column, coupled to the UV-VIS detector, all other substances were calibrated and analysed on the longer column and the refractive index detector.

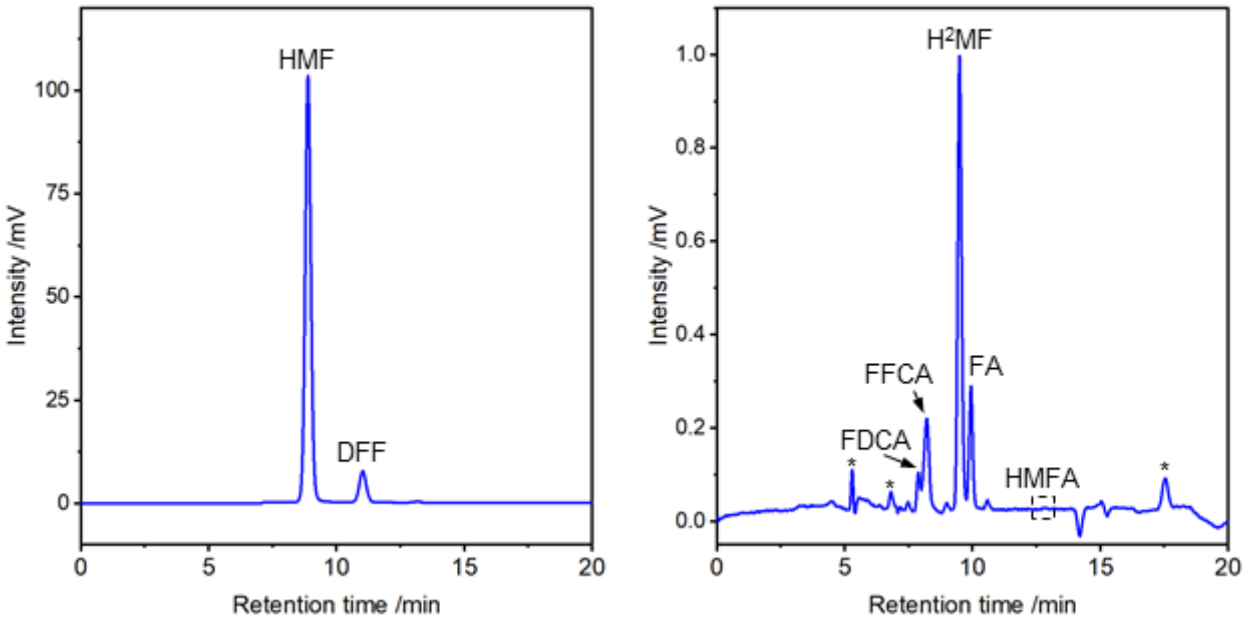

Figure S 17 : Example of HPLC chromatograms (UV-Vis detector left, refractive index detector right) after photocatalysis. Unknown product peaks are indicated with *.

3.6. IR spectroscopy

DRIFT experiments were measured on a Bruker VERTEX 70 spectrometer with a Harrick Scientific praying mantis in a range between 850-4500 cm^{-1} (MCT detector, resolution 1 cm^{-1}). Prior to the DRIFT experiments the samples were degassed inside the high temperature reaction chamber for 30 min under nitrogen atmosphere at 150 °C.

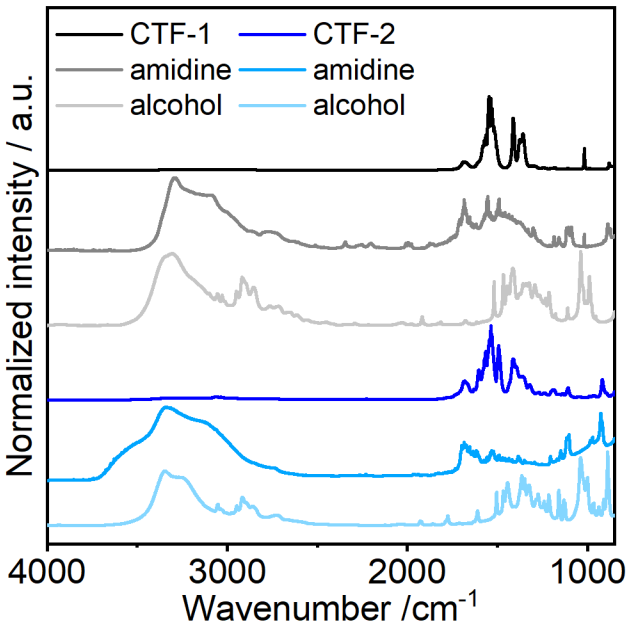

Figure S 18 : DRIFTS of the CTFs and the corresponding amidine hydrochloride monomers.

3.7. Mass spectrometry

Chemical ionization mass spectra in methane were recorded with a Finnigan SSQ 7000 using a direct insertion probe at the institute of organic chemistry at RWTH Aachen.

3.8. NMR spectroscopy

Liquid 1D and 2D NMR experiments were performed on a Bruker Ascend 400 MHz device with TopSpin software automation. Solid-state ^{13}C HPDEC MAS-NMR was performed on a 500 MHz Bruker Avance III. To all solid-state spectra, a line broadening of 20 Hz was applied. Deconvolution of ^{13}C MAS NMR spectra was done using DMFit.[18]

Table S 6 : Overview of signal position and linewidth as obtained by signal deconvolution using DMFit.[18]

material	triazine signals		aromatic signals		
CTF-1	169 ppm (490 Hz)	164 ppm (670 Hz)	138 ppm (470 Hz)	127 ppm (560 Hz)	
CTF-2	169 ppm (620 Hz)	162 ppm (790 Hz)	133 ppm (550 Hz)	128 ppm (620 Hz)	123 ppm (540 Hz)

3.9. Physisorption experiments

The ASAP 2060 device from micromeritics was used for N_2-physisorption experiments at 77 K. All samples were degassed at 150 °C before the measurement. The software MicroActive assisted data evaluation such as total pore volume determination BET and DFT modelling Note that we used here a DFT model developed for rigid carbon with slit pore geometry (HS-2D-NLDFT, carbon, N_2@77), taking into account energetical heterogeny and geometrical corrugation of the carbon surface, but not considering any heteroatoms. As the CTFs contain a lot of heteroatoms (H, N), the pore size distributions obtained from the DFT model should be seen as a rough estimation. Single point total pore volume was obtained for the volume adsorbed at the relative pressure p/p_0 = 0.95.

H_2O vapour physisorption isotherms were recorded on a Quantachrome Autosorb iQ at 298 K to study the interactions of the materials with the solvent used in catalysis. The water vapour isotherms of both materials are characterised by a strong hysteresis over the entire pressure range, indicative for a swelling of the porous network (Fig. S20 left). CTF-1 possesses high initial slope of the isotherms, while the uptake of water vapour is significant less steep in CTF-2. This is also reflected by a Henry constant approx. one order in magnitude lower for CTF-2 (Fig. S20 right). The Henry constant is an indicator for the affinity of the material's surface to water vapour. Thus CTF-1 is the more hydrophilic material which is also reflected by its high total water uptake.

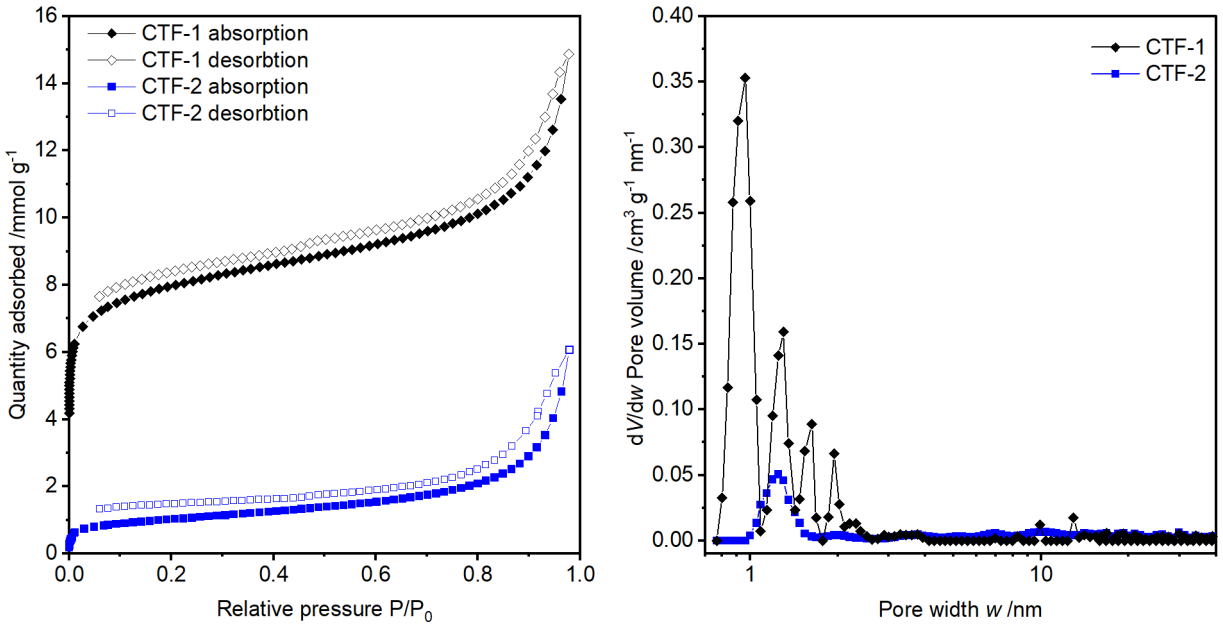

Figure S 19: N_2-Physisorption isotherm (left) of CTF-1 (black) and CTF-2 (blue) at 77 K and estimated pore size distributions (right) for CTF-1 (black) and CTF-2 (blue) assuming cylindrical pores.

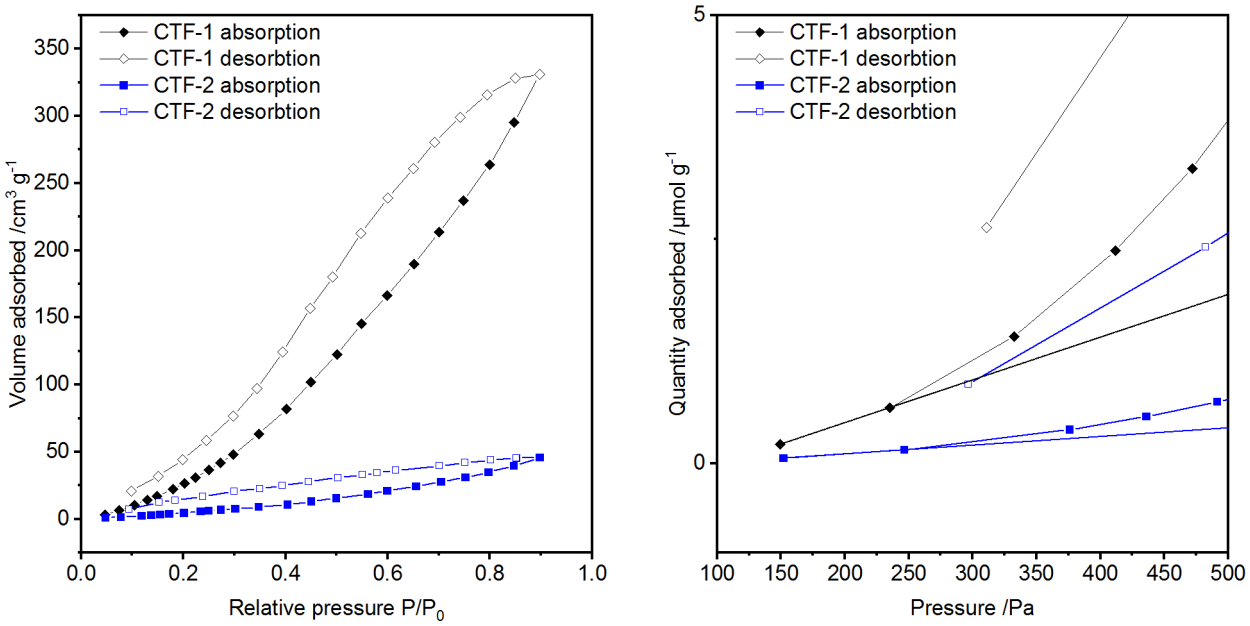

Figure S 20: H_2O-Physisorption isotherm of CTF-1 (black) and CTF-2 (blue) at 298 K (left) and cut out of quantity adsorbed at absolute pressure to determine the Henry constante K_H .

Table S 7 : Overview of surface polarity of CTF-1 and CTF-2.

material	K_H / µmol g^{-1} Pa^{-1}
CTF-1	4.8 ·10^{-3}
CTF-2	0.97 ·10^{-3}

3.10. pXRD analysis

Powder X-ray diffractometry was performed with a Bruker second generation D2 Phaser equipped with a LynxEye XE-T detector and a Cu K_α source. Measurements were conducted from 6 to 90° with 0.02° and 0.4s per step. Smaller angles from 2° to 90° (0.015° and 120 s per step) in 1 mm capillaries in Debye-Scherrer geometry could be measured in transmission on a Stoe Stadi P device with a Mythen1K Detector and a Cu K_α source. The simulated spectra are based on the optimized geometry of section SI 1.3 DFT and simplified TD-DFT calculations.

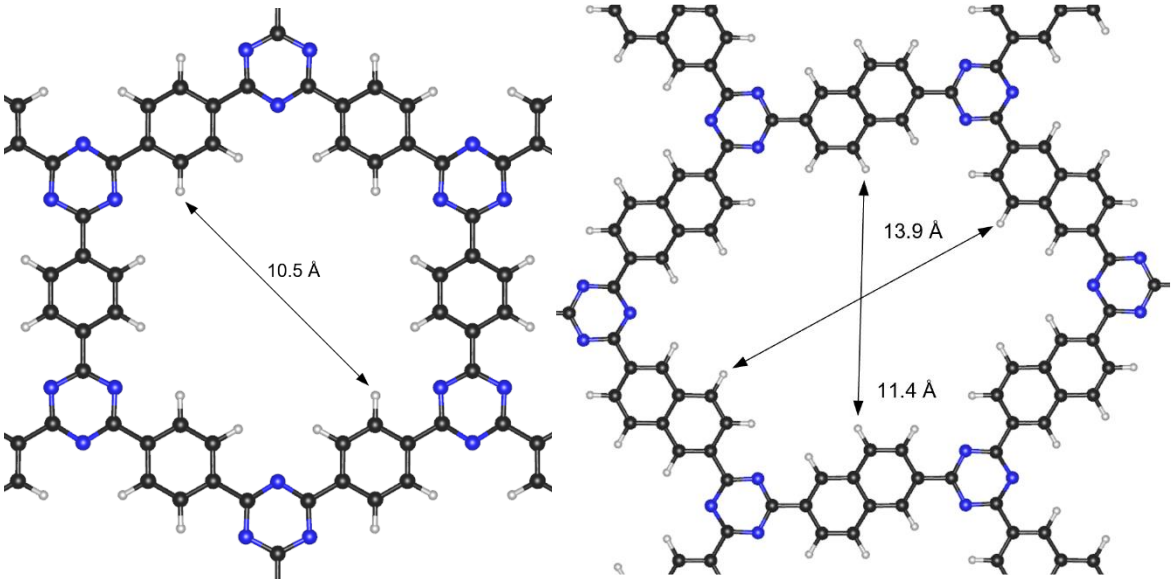

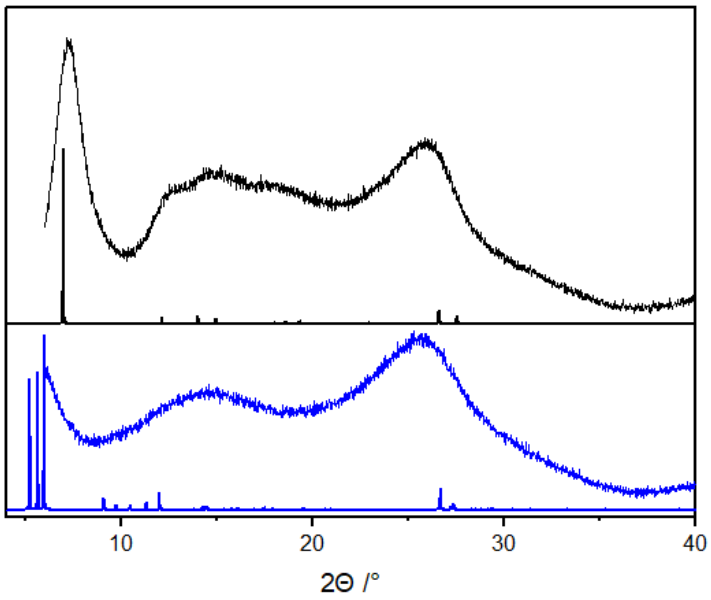

Figure S 21: (top) Idealized CTF-1 and -2 structure after geometry optimization; (bottom) experimental and simulated diffractogram of CTF-1 (black) and CTF-2 (blue).

3.11. Pair Distribution Function measurements

Powder XRD data for pair distribution function (PDF) analysis was collected with a STOE STADI P diffractometer, equipped with a Dectris MYTHEN2 4K detector using Ag $K\alpha_1$ radiation. A powder sample of CTF-1 was measured for 48 hours in a borosilicate glass capillary of 0.5 mm diameter, using a Q-range of 0.4 - 19.3 $Å^{-1}$ for data processing. For calculating the G(r) function, xPDFsuite was used, subtracting the capillary contribution during PDF calculation. The XRD pattern, I(Q), after capillary subtraction and the resulting PDF can be seen in Fig S23 panel A and B, respectively. In the PDF, we can clearly identify interatomic distances of local structural motifs (panel C).

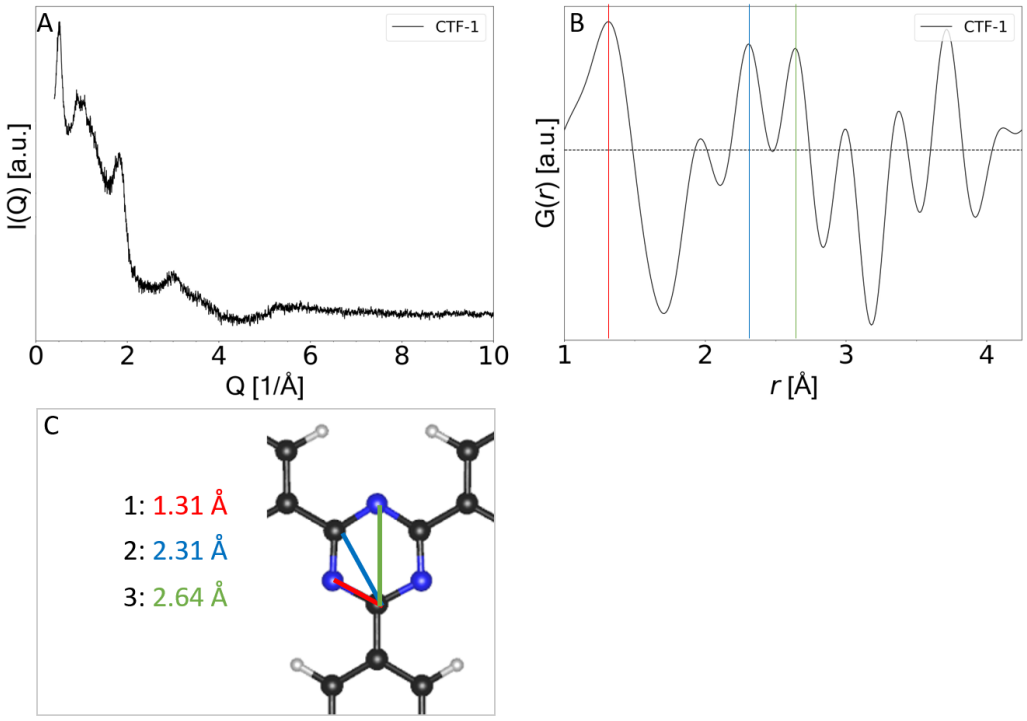

Figure S 22: (A) XRD pattern of CTF-1 after subtraction of empty capillary. (B) Resulting PDF with baseline (dashed line) at 0. Interatomic distances visible in the PDF can be allocated to (C) the local structure as highlighted in different colors.

3.12. Radiant flux density

The radiant flux density was measured with a HD 2102.2 photo-radiometer from DeltaOhm equipped with a LP 471 UVA or a LP 471 RAD probe.

3.13. SEM

Scanning electron microscopy was performed with a COXEM EM-30 benchtop SEM. Therefore, some CTF was placed on a sample holder with carbon tape and gently pressed down with a spatula to increase adhesion. All samples were sputter coated with Au (COXEM SPT-20, 7 A ,180 s, approx. 20 nm layer).

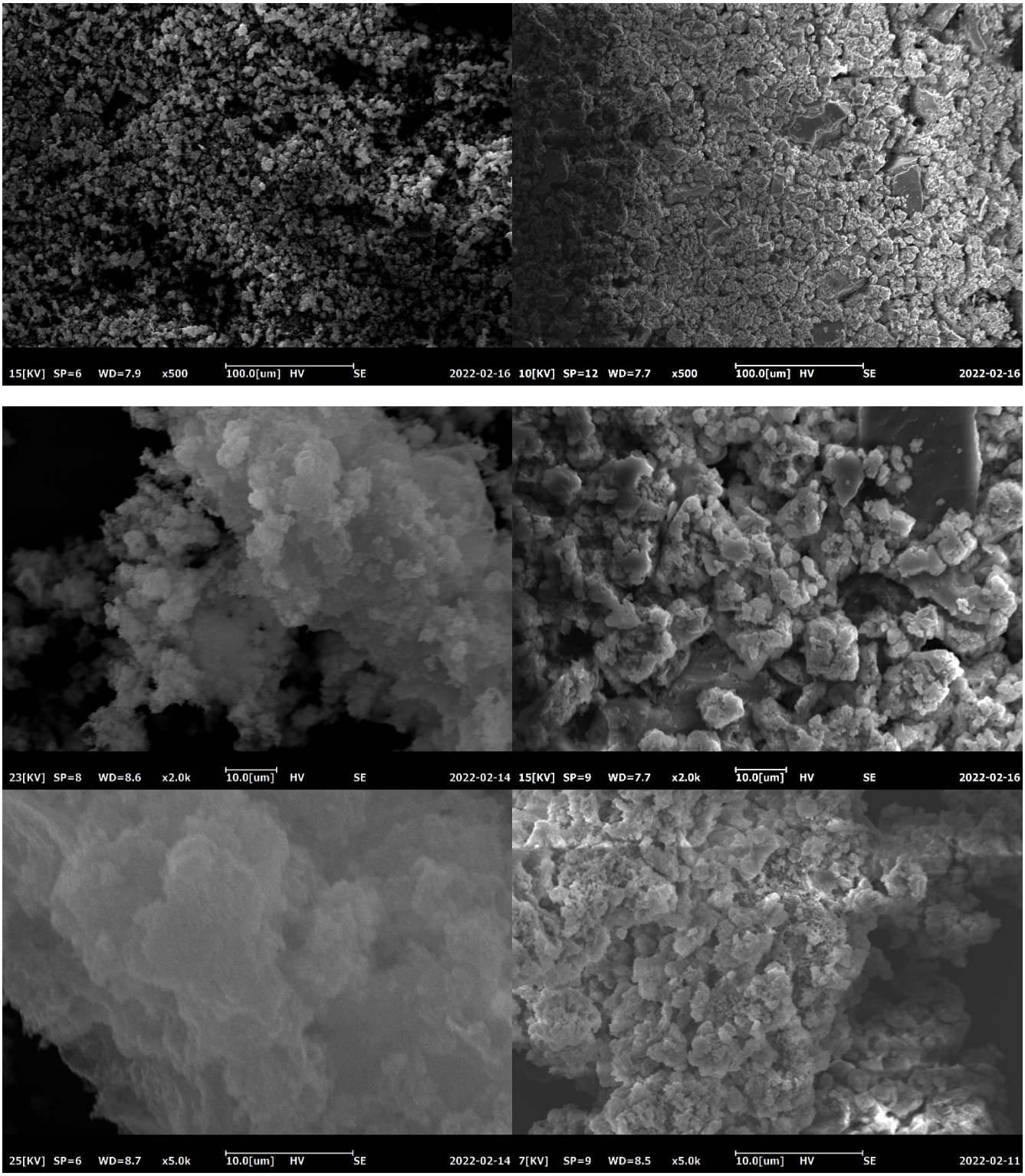

Figure S 23: SEM images of CTF-1 (left) and CTF-2 (right) at different magnifications.

3.14. UV Vis spectroscopy

UV-VIS diffuse reflectance spectroscopy of the undiluted photocatalysts was measured with a Lambda 7 spectrometer from PerkinElmer with the respective accessory in the range of 320 to 700 nm against $BaSO_4$ as standard. The PerkinElmer UV-Winlab 2.80.03 software package was used for measurement control and data analysis. The band gap was determined via the Tauc-plot method for direct and indirect transitions.[19]

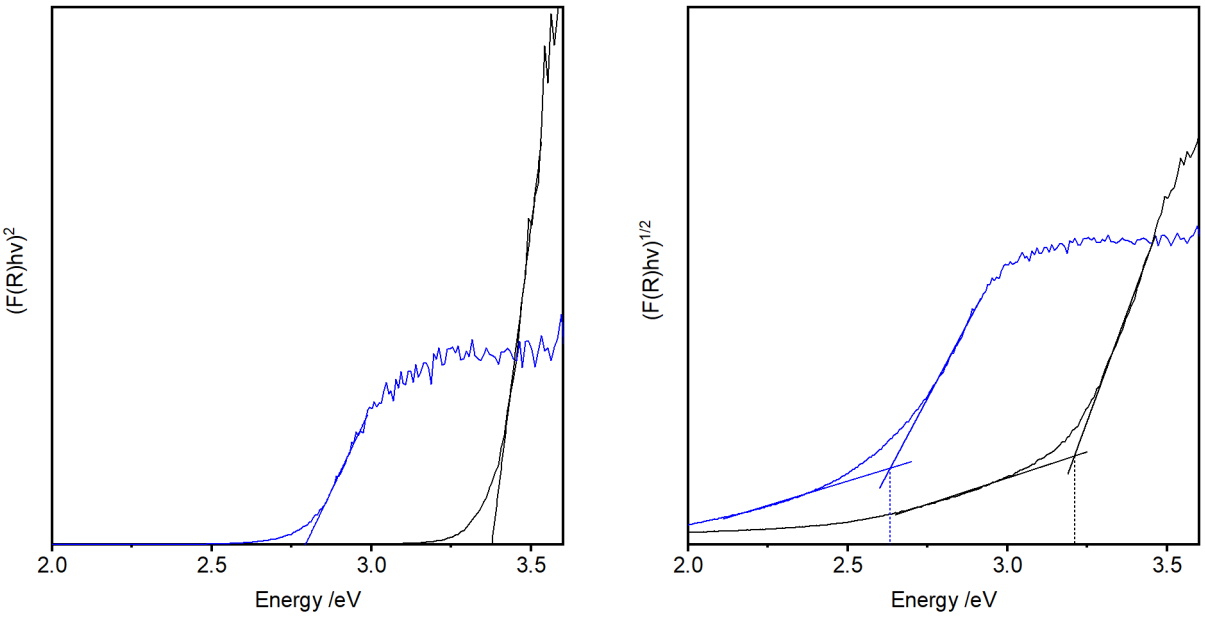

Figure S 24: Tauc plot for direct transitions (left) and indirect transitions (right) for CTF-1 (black) and CTF-2 (blue).

4. References

[1] a) Kresse, Hafner, *Phys. Rev. B* **1994**, *49*, 14251; b) G. Kresse, J. Furthmüller, *Comput. Mater. Sci.* **1996**, *6*, 15.
[2] Perdew, Burke, Ernzerhof, *Phys. Rev. Lett* **1996**, *77*, 3865.
[3] S. N. Steinmann, C. Corminboeuf, *J. Chem. Theory Comput.* **2011**, *7*, 3567.
[4] a) Blöchl, *Phys. Rev. B* **1994**, *50*, 17953; b) G. Kresse, D. Joubert, *Phys. Rev. B* **1999**, *59*, 1758.
[5] H. J. Monkhorst, J. D. Pack, *Phys. Rev. B* **1976**, *13*, 5188.
[6] Blöchl, Jepsen, Andersen, *Phys. Rev. B* **1994**, *49*, 16223.
[7] C. Bannwarth, S. Ehlert, S. Grimme, *J. Chem. Theory Comput.* **2019**, *15*, 1652.
[8] "Semiempirical Extended Tight-Binding Program Package (version 6.4.0)", can be found under https://github.com/grimme-lab/xtb, **2022**.
[9] a) T. Risthaus, A. Hansen, S. Grimme, *Phys. Chem. Chem. Phys.* **2014**, *16*, 14408; b) S. Grimme, *J. Chem. Phys.* **2013**, *138*, 244104.
[10] a) F. Weigend, R. Ahlrichs, *Phys. Chem. Chem. Phys.* **2005**, *7*, 3297; b) J.-D. Chai, M. Head-Gordon, *J. Chem. Phys.* **2008**, *128*, 84106.
[11] "stda program for computing excited states and response functions via simplified TD-DFT methods (version 1.6.2)", can be found under https://github.com/grimme-lab/stda, **2022**.
[12] S. Seritan, C. Bannwarth, B. S. Fales, E. G. Hohenstein, C. M. Isborn, S. I. L. Kokkila-Schumacher, X. Li, F. Liu, N. Luehr, J. W. Snyder et al., *Wiley Interdiscip. Rev.-Comput. Mol. Sci.* **2021**, *11*, U426.
[13] M. Liu, Q. Huang, S. Wang, Z. Li, B. Li, S. Jin, B. Tan, *Angew. Chem. Int. Ed.* **2018**, 11968.
[14] H. Gielen, C. Alonso-Alija, M. Hendrix, U. Niewöhner, D. Schauss, *Tetrahedron Lett.* **2002**, *43*, 419.
[15] J. R. Lakowicz, Principles of fluorescence spectroscopy, Springer, New York, 2006.

[16] M. Pastorczak, M. Kozanecki, J. Ulanski, *J. Phys. Chem. A* **2008**, *112*, 10705.
[17] Q. Hu, H. Zhao, S. Ouyang, *Phys. Chem. Chem. Phys.* **2017**, *19*, 21540.
[18] D. Massiot, F. Fayon, M. Capron, I. King, S. Le Calvé, B. Alonso, J.-O. Durand, B. Bujoli, Z. Gan, G. Hoatson, *Magn. Reson. Chem.* **2002**, *40*, 70.
[19] P. Makuła, M. Pacia, W. Macyk, *J. Phys. Chem. Lett.* **2018**, *9*, 6814.